Topology of coherent precession in superfluid ^{3}He-B

T. Sh. Misirpashaev and G. E. Volovik

Landau Institute for Theoretical Physics of Russian Academy of Sciences;
Low Temperature Laboratory, Helsinki University of Technology, Finland
(Submitted 9 April 1992)
Zh. Eksp. Teor. Fiz. **102**, 1197–1227 (October 1992)

Coherently precessing states in ^{3}He-B are considered within the general formalism of broken symmetry. A 6-dimensional manifold of Larmor precession is found instead of the 4-dimensional space of conventional stationary ^{3}He-B. The degeneracy states are described by two rotational matrices instead of one matrix $R_{\alpha i}$ of the stationary B-phase states. The nontrivial topology of the extended space together with the hierarchy of interactions and length scales gives rise to a variety of new topologically stable objects. Continuous and discrete symmetries of the Lagrangian describing the spin dynamics are discussed, which lead to a relation between the properties of the precessing and stationary states.

INTRODUCTION

The coherent spin precession in superfluid ^{3}He-B has proven to be extremely stable, as was found in Refs. 1–4. The unique properties of the precessing state, usually referred to as the homogeneously precessing domain (HPD), have been applied to the investigation of the superfluid ^{3}He-B, in particular of the topological defects in superfluid ^{3}He-B which appear under rotation. The HPD technique allows one to prove the breaking of the axial symmetry in the cores of quantized vortices[5] and to observe the combined spin-current and mass-current vortex, which has a soliton tail.[6]

Here we discuss the topological objects which can arise in addition to the Larmor precession. Until now only one such object has been described[7,8] and observed.[9] This is the line about which the winding of the phase of the spin precession takes place. We show that a variety of other topological objects is possible, and they are classified essentially by the same homotopy topology method as the topological defects in the stationary condensed matter (see the reviews in Refs. 10–13).

This application of the topological methods is possible because the state precessing with the frequency close to the Larmor frequency, belongs to the class of ordered time-dependent coherent states, which is a generalization of the conventional stationary coherent state described by the order parameter. The precessing states also have a stiffness (or rigidity), which is the main feature of the ordered state with broken symmetry. Therefore the topological analysis of the time-dependent coherent states is in many respects analogous to that of the stationary superfluid phases of ^{3}He. It is not necessary to solve the Leggett equations of the spin dynamics. Instead it is enough to consider the broken and remaining symmetries of the coherent states, using the Larmor theorem, which shows the equivalence of the effect of the external magnetic field and the effect of precession with the Larmor frequency.

The symmetry approach allows one to obtain the space of the degenerate states, the number of Goldstone bosons (gapless collective modes), the possible topological defects, etc. In the same manner as for the stationary states, an ordering of the energies takes place which leads to reduction of the manifold of internal states at different length scales. They cause the orientation of the order parameter to be partly or completely fixed. This produces gaps in the spectrum of collective modes and gives rise to additional topological objects (textures and solitons), described by the relative homotopy groups.

The most important is the dipole-dipole spin-orbit interaction. It reduces the multi-dimensional space of the Larmor precession to two separate subspaces: the non-precessing stationary state (NPD: Non-Precessing Domain) and the pure homogeneously precessing state which has been observed experimentally (HPD: Homogeneously Precessing Domain). These states reveal many similar features which result from the discrete symmetry relating them. This symmetry is violated by other interactions: the spectroscopic energy which is proportional to the deviation of the external frequency ω from the Larmor frequency, the interaction of the order parameter with the mass current, surface energy, etc.

In Sec. 1 we repeat the general symmetry approach for the stationary superfluid states of ^{3}He-B in order to generalize this for the Larmor precession states in Sec. 2, where we find the extension of the conventional 4-dimensional manifold of internal states to the 6-dimensional manifold. In Sec. 3, the orientation energies are introduced for the extended order parameter, which gives the hierarchy of energy and length scales. In Sec. 4 the topological object related to the short length scale (less than the dipole length) are discussed; in addition to the conventional mass-current and spin-current vortices the topologically stable point defects are found—the hedgehogs in the fields of the spin and orbital angular momenta. Section 5 is devoted to the defects resulting from the topology at distances larger than the dipole length and from the interplay of different length scales. Present among them is the intersection line of several interfaces between the HPD and NPD, which is described by the nontrivial elements of the fundamental homotopy group. In Sec. 6 the topological defects on the length scale where the spectroscopic energy becomes important are discussed. And finally, the core structure of the hedgehog is discussed in Sec. 7, where the phase-slip process is found which is regulated by the homotopy group π_3. In Sec. 8 the application of the method to the precessing states in other superfluid phases is discussed. In the Appendix the Lagrangian is considered which gives the Leggett equations of the spin dynamics, and the symmetry properties of the Lagrangian related to the Larmor theorem are discussed including the local gauge in-

 0038-5646/92/100650-16$05.00

variance. The discrete symmetry of the Lagrangian is discussed which leads to mapping of the properties of the HPD states to those of the NPD, including the spectrum of the collective modes, which appears to be similar for the precessing and the corresponding stationary states.

1. BROKEN RELATIVE SYMMETRY IN THE STATIONARY ^{3}He-B SUPERFLUID

The relevant symmetry group G of the physical laws, which is broken in superfluid phases of ^{3}He, contains the gauge group $U(1)$ and the group of rotations. Since the spin-orbit (dipole-dipole) interaction is relatively weak, the spin and orbital rotation groups, SO_3^S, and SO_3^L, can be considered independently:

$$G=U(1)\times SO_3{}^L\times SO_3{}^S. \tag{1.1}$$

The superfluid phases of ^{3}He are distinguished by their remaining symmetry H. The equilibrium state of the phase B is invariant under combined spin and orbital rotations, while the separate rotations transform the initial state into another degenerate equilibrium state with different order parameter.

The simplest equilibrium state of the B-phase, which can be chosen as the initial state, corresponds to the total angular momentum $J=0$, which means that this order parameter is invariant under simultaneous and equal spin and orbital rotations:[14]

$$A_{\alpha i}^{(0)}=\Delta_B\delta_{\alpha i}. \tag{1.2}$$

If $\hat{R}^{(1)}$ and $\hat{R}^{(2)}$ are matrices of spin and orbital rotations respectively, and $e^{i\Phi}$ is the operation of the gauge transformation, then the B-phase state described by the order parameter (1.2) is transformed under operations of the symmetry G into another degenerate B-phase state described by the following order parameter:

$$A_{\alpha i}=e^{i\Phi}R_{\alpha\beta}^{(1)}R_{ik}^{(2)}A_{\beta k}^{(0)}=\Delta_B e^{i\Phi}R_{\alpha i}, \tag{1.3}$$

where the conventional $\hat{R}$ matrix of the B-phase is expressed in terms of $\hat{R}^{(1)}$ and $\hat{R}^{(2)}$ as

$$\hat{R}=\hat{R}^{(1)}(\hat{R}^{(2)})^{-1}. \tag{1.4}$$

It is important that the state described by the $\hat{R}$ matrix does not resolve between $\hat{R}^{(1)}$ and $\hat{R}^{(2)}$, which is the essence of the broken relative invariance.[15] Only relative rotations lead to a new equilibrium state, while the combined rotations with $\hat{R}^{(1)}=\hat{R}^{(2)}$ leave the $\hat{R}$ matrix unmoved. Thus the space R of the degenerate states of the B-phase includes the circumference $U(1)$ of the phase Φ and the SO_3^{rel} space of the $\hat{R}$ matrix:

$$R=U(1)\times SO_3{}^{rel}. \tag{1.5}$$

The orthogonal $\hat{R}$ matrix can be specified by the angle θ and the rotation axis $\hat{n}$

$$R_{\alpha i}(\hat{n},\theta)=\hat{n}_\alpha\hat{n}_i+(\delta_{\alpha i}-\hat{n}_\alpha\hat{n}_i)\cos\theta-e_{\alpha ik}\hat{n}_k\sin\theta. \tag{1.6}$$

The spin-orbit interaction

$$F_D={}^2/_{15}\chi_B\Omega_L{}^2(\mathrm{Tr}\,\hat{R}-{}^1/_2)^2={}^8/_{15}\chi_B\Omega_L{}^2(\cos\theta+{}^1/_4)^2 \tag{1.7}$$

fixes the θ angle, $\cos\theta_0=-\frac{1}{4}$, but leaves the degeneracy with respect to the orientation of $\hat{n}$. (Ω_L is the so called Leggett frequency, the frequency of the longitudinal NMR, and χ_B is the spin susceptibility of the ^{3}He-B. We use the system of units in which the gyromagnetic ratio γ for the ^{3}He atom is 1, so the magnetic field and the frequency will have the same physical dimension.) Thus the space R of the degenerate states of the B-phase is reduced by the dipole interaction to

$$R_D=U(1)\times S^2, \tag{1.8}$$

where S^2 is the sphere of the $\hat{n}$ vector.

The homotopy groups of the spaces R and R_D [$\pi_1(R,R_D)$ and $\pi_2(R,R_D)$] lead to the topologically stable defects of the stationary B-phase: quantized mass-current vortices, spin disclinations, θ solitions and $\hat{n}$ hedgehogs.[10-13]

2. EXTRA BROKEN SYMMETRY IN THE COHERENT PRECESSION STATES OF SUPERFLUID ^{3}He-B

Let us consider now the time-dependent coherent states which appear not under stationary external conditions but under external time-dependent fields. Now the state is a matrix-valued function of time $A_{\alpha i}(t)$ instead of a constant matrix in the stationary case. The symmetry group of physical laws acts on the functions $A_{\alpha i}(t)$ and can in principle contain time-dependent operators $g(t)$ from the group

$$U(1)(t)\times SO_3{}^L(t)\times SO_3{}^S(t) \tag{2.1}$$

of time-dependent gauge transformations and orbital and spin rotations. Whether the time-dependent symmetries are allowed depends on the form of the Hamiltonian. We will see that in the case of nonlinear NMR where the coherently precessing states arise under a constant magnetic field $\mathbf{H}_0$ and a small radio frequency (rf) field $\mathbf{H}_{rf}(\omega t)\perp\mathbf{H}_0$, with the frequency ω being close to the Larmor frequency $\omega_L=H_0$, the Larmor theorem provides the existence of such symmetries.

2.1. Symmetry and the order parameter at short distance (spin-orbit interaction neglected)

The ^{3}He is electrically neutral, so the magnetic field $\mathbf{H}_0$ interacts only with the spin of the ^{3}He atom: the Larmor energy is $F_L=-\mathbf{H}_0\cdot\mathbf{S}$. The field $\mathbf{H}_0$ produces an anisotropy in the spin space along the field, which leads to the reduction of the group G of the physical laws in the presence of an external magnetic field: instead of SO_3^S one has SO_2^S. However the SO_3 spin rotation symmetry is restored if we consider the experimentally relevant particular case when the rf frequency is close to the Larmor frequency $\omega_L=H_0$ and is larger than the Leggett frequency: $\omega-\omega_L\ll\omega_L$, $\Omega_L\ll\omega_L$. So to lowest order one has $\omega=\omega_L$ and also the spin-orbit interaction can be neglected. We will not take into account the dissipative terms, assuming that the amplitude H_{rf} is maintained large enough to balance the dissipation of energy in the precessing state. However, $H_{rf}\ll H_0$, holds, and we will always neglect the amplitude H_{rf} of the rf field, supposing that the rf field only fixes the precession frequency ω. In this situation one can apply the powerful Larmor theorem. According to this theorem, in the spin-space coordinate frame rotating with the frequency $\boldsymbol{\omega}=\mathbf{H}_0$ the effect of the magnetic field $\mathbf{H}_0$ on the spins of the ^{3}He atoms completely disappears. The Zeeman energy $F_L=-\mathbf{H}_0\cdot\mathbf{S}$ is balanced by the Larmor energy term $\boldsymbol{\omega}\cdot\mathbf{S}$ which appears in the rotating spin frame.

Since in the rotating spin frame the magnetic field becomes irrelevant, the spin rotation symmetry is restored, but now in the spin-precessing frame. Therefore the total symmetry group of the physical laws is now

$$\tilde{G} = U(1) \times SO_3^L \times SO_3^{\tilde{S}}, \tag{2.2}$$

where $SO_3^{\tilde{S}}$ is the group of spin rotations in the rotating frame. The elements $\tilde{g}(t)$ of the group $SO_3^{\tilde{S}}$ are constructed from the elements g of the conventional SO_3^S group in the following way:

$$\tilde{g}(t) = \hat{O}^{-1}(\hat{z}, \omega t) g \hat{O}(\hat{z}, \omega t), \tag{2.3}$$

where the orthogonal matrix

$$O_{\alpha\beta}(\hat{z}, \omega t) = (\hat{O}^{-1})_{\alpha\beta}(\hat{z}, -\omega t)$$

$$= \hat{z}_\alpha \hat{z}_\beta + (\delta_{\alpha\beta} - \hat{z}_\alpha \hat{z}_\beta) \cos \omega t - e_{\alpha\beta\gamma} \hat{z}_\gamma \sin \omega t$$

is the transformation from the laboratory frame into the rotating frame—this is a rotation about the z axis (along H_0) through the angle ωt. The Eq. (2.3) means that to perform the $SO_3^{\tilde{S}}$ symmetry transformation one should first make the transformation from the laboratory frame into the precessing frame, then perform the $\hat{R}^{(1)}$ rotation within this frame, and after that return to the laboratory frame. $\tilde{G}$ is the symmetry group of the Lagrangian which defines the dynamics of the system (see Appendix A) if the spin-orbit coupling is neglected.

The group $\tilde{G}$ is isomorphic to the large symmetry group G of the physical laws in Eq. (1.1), which holds in the absence of the magnetic field and under stationary conditions. This isomorphism reflects the Larmor theorem, which implies the equivalence of the magnetic field and spin precession with the Larmor frequency: if the spin-orbit interaction is absent the physics should be the same.

Now we can find all the degenerate coherent states of the Larmor precession by applying the symmetry group (2.2) to some simple state. It is evident that the stationary (NPD) state (1.2) with the equilibrium spin density $\mathbf{S}^{(0)} = \chi_B \mathbf{H}_0$ is one of these states. So we take this state as the simplest initial state

$$A_{\alpha i}^{(0)} = \Delta_B \delta_{\alpha i}, \quad \mathbf{S}^{(0)} = \chi_B \mathbf{H}_0. \tag{2.4}$$

The action of elements of $\tilde{G}$ on this state $\hat{A} = \hat{O}^{-1} \hat{R}^{(1)} \hat{O} \hat{A}^{(0)} (\hat{R}^{(2)})^{-1}$ leads to the following general coherent B-phase state under the rf field with the Larmor frequency, neglecting the spin-orbit interaction

$$A_{\alpha i}(t) = \Delta_B e^{i\Phi} R_{\alpha i}(t),$$

$$R_{\alpha i}(t) = O_{\alpha\beta}(\hat{z}, -\omega t) R^{(1)}_{\beta\gamma} O_{\gamma\mu}(\hat{z}, \omega t) (R^{(2)})^{-1}_{\mu i}. \tag{2.5}$$

The spin density in this state is also obtained by the spin rotation $SO_3^{\tilde{S}}$ from the initial spin in Eq. (2.4):

$$S_\alpha(t) = O_{\alpha\beta}(\hat{z}, -\omega t) R^{(1)}_{\beta\gamma} \chi_B H_{0\gamma}. \tag{2.6}$$

This means that the spin density in the precessing frame, $\tilde{S}_\beta$, is constant in time:

$$\tilde{S}_\beta = O_{\beta\alpha}(\hat{z}, \omega t) S_\alpha(t) = \chi_B R^{(1)}_{\beta\gamma} H_{0\gamma}, \tag{2.7}$$

which corresponds to the precession of spin with the tipping angle

$$\cos \beta_1 = \frac{\tilde{\mathbf{S}} \cdot \mathbf{H}_0}{\chi_B H_0^2} = R^{(1)}_{zz}. \tag{2.8}$$

One can check that Eqs. (2.5), (2.6) represent the general solution of the spatially homogeneous Leggett equations describing the spin dynamics (See Appendix B), under the conditions that $\omega = \omega_L$ and that the spin-orbit interaction is absent.

So the general coherent state of the Larmor precession contains as the degeneracy parameters the phase Φ of the Bose condensate and the two rotation matrices $\hat{R}^{(1)}$ and $\hat{R}^{(2)}$. As distinct from the coherent states in Eqs. (1.3)–(1.4) under stationary conditions, these two rotations occur in the precessing and laboratory systems respectively, and therefore they cannot compensate each other. So both matrices represent degeneracy parameters.

Note that the $\hat{R}^{(1)}$ matrix has only spin indices, while $\hat{R}^{(2)}$ in Eq. (2.5) has both spin and orbital indices. This is important for the construction of the interaction terms in Sec. 3. The physical meaning of these matrices is as follows: the $\hat{R}^{(1)}$ matrix defines the orientation of the spin in the precessing frame according to Eq. (2.7), while the $\hat{R}^{(2)}$ matrix defines the orientation of the orbital momentum $L_i = -R_{\alpha i}(t) S_\alpha(t)$. This momentum is constant in the laboratory frame according to the following equation:

$$L_i = -R_{\alpha i}(t) S_\alpha(t) = -\chi_B R^{(2)}_{\alpha i} H_{0\alpha}. \tag{2.9}$$

The direction of $\mathbf{L}$ also shows the orbital anisotropy axis for the gap in the quasi-particle energy spectrum. Moreover, we shall use the unit vector $\hat{l} = -\mathbf{L}/\chi_B H_0$ for the axis of the orbital anisotropy.

This orbital anisotropy is usually small since we have $\omega_L \ll \Delta_B$, but it can be incorporated in the general formalism if one takes into account in the initial stationary B-phase state in Eq. (2.4):

$$A_{\alpha i}^{(0)} = \Delta_\perp \delta_{\alpha i} + (\Delta_\parallel - \Delta_\perp) \hat{z}_\alpha \hat{z}_i, \quad \mathbf{S}^{(0)} = \chi_B H_0 \hat{z}.$$

Here $\Delta_\parallel$ and $\Delta_\perp$ are gaps in the quasiparticle spectrum for the momenta parallel and perpendicular to $\hat{z}$ with $(\Delta_\perp - \Delta_\parallel)/\Delta_\perp \sim \omega_L^2/\Delta_B^2$. The $\hat{R}^{(2)}$ matrix rotates this axis to obtain the anisotropy axis $\hat{l} = \hat{R}^{(2)} \cdot \hat{z}$ for the general state.

One can see now that not only the relative symmetry but also the combined symmetry is spontaneously broken in such coherent states. Even if one takes $\hat{R}^{(1)} = \hat{R}^{(2)}$ one obtains a degenerate coherent state which is different from the initial one, since $\tilde{\mathbf{S}}$ and $\mathbf{L}$ are oriented differently. It is important that the combined symmetry is not broken completely. Some symmetry still remains: the rotations induced by matrices $\hat{R}^{(1)}$ and $\hat{R}^{(2)}$ about the axis z can compensate each other. Therefore the symmetry subgroup of the coherent state is

$$\tilde{H} = SO_2^{J_z}, \tag{2.10}$$

where the rotation group $SO_2^{J_z}$ is the symmetry of the state under simultaneous spin and orbital rotation about the axis z. The factorization over the invariant subgroup leads to the manifold of degenerate states

$$\tilde{R} = \tilde{G}/\tilde{H} = U(1) \times (SO_2^L \times SO_3^{\tilde{S}})/SO_2^{J_z} = U(1) \times SO_3 \times S^2. \tag{2.11}$$

As a result we have a topologically nontrivial 6-dimen-

sional space of degenerate states—the most complicated space known in condensed matter (the same space of degenerate states could occur in the stationary planar phase of ^{3}He if this phase were stable). This $D=6$ space of coherent states includes the conventional 4-dimensional manifold (1.5) of the stationary B-phase states as its subspace, this subspace R of $\tilde{R}$ can be obtained if one takes $\hat{R}^{(1)}$ as the unit matrix.

A convenient parametrization for five independent variables of the matrices $\hat{R}^{(1)}$ and $\hat{R}^{(2)}$ can be made in terms of the Euler angles: $\hat{R}^{(1)}(\alpha_1,\beta_1,\gamma_1)$ with α_1 and β_1 being the azimuthal and polar angles of $\hat{s}=\tilde{\mathbf{S}}/S$ and $\hat{R}^{(2)}(\alpha_2,\beta_2,\gamma_2)$ with α_2 and β_2 being the azimuthal and polar angles of the orbital vector $\hat{l}$. Due to the combined symmetry the state is defined by 5 variables: $\hat{s}(\alpha_1,\beta_1)$, $\hat{l}(\alpha_2,\beta_2)$ and the relative rotation about the z axis by the angle $\gamma=\gamma_1-\gamma_2$.

In the traditional states with broken symmetry the 6-dimensional space of the degenerate states would result in the existence of six Goldstone (gapless, or low-frequency) collective modes. The situation is different in the presence of the magnetic field due to the absence of the time reversal symmetry. On the one hand the Larmor gap ω_L appears for some of the collective modes. On the other hand the oscillation with frequency close to ω_L corresponds to the low-frequency motion in the precessing frame. Therefore the modes with the frequency close to ω_L can also be considered as Goldstone modes. In our case the low frequency oscillations of $\hat{s}$ represent the Goldstone mode in the precessing frame, while in the laboratory frame this is the mode with the frequency close to ω_L. Such oscillations superposed on the stationary state correspond to the transverse NMR mode. The low-frequency oscillations of γ correspond to the longitudinal NMR mode in the stationary state. And finally the low frequency oscillations of the orbital vector $\hat{l}$ represent the Goldstone mode in the laboratory frame, which we will refer to as orbital waves. In the stationary state this corresponds to the gapless branch of the transverse NMR. The spectrum of the modes is discussed in Appendix D; the symmetry Z_2 of the Lagrangian is used to relate the spectrum superposed on the NPD to that of the HPD found by Fomin.[16,17]

2.2. The order parameter space at large distance (spin-orbit taken into account)

The 6-dimensional manifold of degenerate states is reduced if the spin-orbit interaction (dipole forces) in Eq. (1.7) is taken into account as a small perturbation of the Larmor precession. After averaging over the basic solution (2.5) for the Larmor precession one obtains the dipole energy in terms of the degeneracy parameters:

$$F_D = {}^2/_{15}\chi_B\Omega_L^2\,[(\hat{s}_z\hat{l}_z - {}^1/_2 + {}^1/_2(1+\hat{s}_z)(1+\hat{l}_z)\cos\gamma)^2 + {}^1/_8(1-\hat{s}_z)^2(1-\hat{l}_z)^2 + (1-\hat{s}_z^2)(1-\hat{l}_z^2)(1+\cos\gamma)], \tag{2.12}$$

where $\hat{s}_z=\cos\beta_1$ and $\hat{l}_z=\cos\beta_2$ are z projections of $\hat{s}$ and $\hat{l}$.

The dipole energy is minimized when either $\hat{s}_z=1$ or $\hat{l}_z=1$ holds, which leads to two families of degenerate states. The first of them is the family $\hat{s}_z=1$ of stationary states (NPD). For this family the $\hat{R}^{(1)}$ is fixed, $R^{(1)}_{\beta\gamma}=\delta_{\beta\gamma}$, as well as the spin density $\mathbf{S}=\chi_B\mathbf{H}_0$, while $\hat{R}^{(2)}$ is the matrix of rotations about the $\hat{n}_2$ axis through the angle θ_0, with $\hat{n}_2$ being arbitrary:

$$R^{(2)}_{\alpha i}(\hat{n}_2,\theta_0)=\hat{n}_{2\alpha}\hat{n}_{2i}+(\delta_{\alpha i}-\hat{n}_{2\alpha}\hat{n}_{2i})\cos\theta_0-e_{\alpha ik}\hat{n}_{2k}\sin\theta_0.$$

According to Eq. (2.9) the $\hat{l}$ vector can be arbitrary within the region $\hat{l}_z\geqslant -1/4$.

Another family represents a special class of precessing states, which we call HPD. It has a fixed $\hat{R}^{(2)}$ matrix, $\hat{R}^{(2)}_{\alpha i}=\delta_{\alpha i}$, and therefore a fixed orbital vector $\hat{l}=\hat{z}$, while

$$R^{(1)}_{\alpha i}(\hat{n}_1,\theta_0)=\hat{n}_{1\alpha}\hat{n}_{1i}+(\delta_{\alpha i}-\hat{n}_{1\alpha}\hat{n}_{1i})\cos\theta_0-e_{\alpha ik}\hat{n}_{1k}\sin\theta_0$$

with $\hat{n}_1$ arbitrary. This means that the orientation of the magnetization $\tilde{\mathbf{S}}$ in the precessing frame can be arbitrary within the region $\hat{s}_z\geqslant -1/4$, as follows from Eq. (2.8).

Note the discrete symmetry Z_2 between the spin and orbital vectors $\hat{s}$ and $\hat{l}$ in the dipole energy (2.12); this symmetry is discussed in Appendix A [see Eq. (A11)]. Due to this symmetry the given NPD state ($\hat{R}^{(1)}=1,\hat{R}^{(2)}=\hat{R}_0$) is equivalent to the HPD state with $\hat{R}^{(2)}=1$ and $\hat{R}^{(1)}=\hat{R}_0^{-1}$. Therefore some properties of the HPD state can be mapped from that of the corresponding stationary state. In particular the collective mode spectrum superposed on the HPD can be obtained from the spin-wave spectrum of the corresponding NPD (see Appendix D).

Due to the discrete Z_2 symmetry the dipole interaction does not discriminate between these two families: the HPD and the NPD are energetically equivalent to each other. Thus the dipole forces reduce the space $\tilde{R}$ to two spheres of $\hat{n}_{1,2}$ vectors in the HPD and NPD states: the sphere of $\hat{n}_1$ in the precessing domain and the sphere of $\hat{n}_2$ within the NPD. Due to the equivalence of rotations about the axis z in HPD and NPD, these two spheres touch each other at two points $\hat{n}_1=\hat{n}_2=\pm\hat{z}$. Therefore the total degeneracy space under the dipole forces is

$$\tilde{R}_D = U(1)\times R(S^2_{\rm HPD},S^2_{\rm NPD}), \tag{2.13}$$

where $R(S^2_{\rm HPD},S^2_{\rm NPD})$ denotes the bundle of two spheres with two equivalent points: the north pole of one sphere is equivalent to the north pole of the other and the same for the south poles (see Fig. 1).

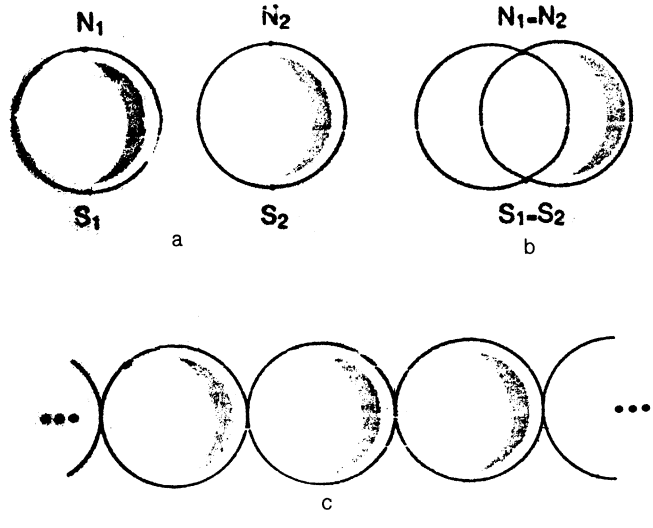

FIG. 1. a,b) Degeneracy space $\tilde{R}_D$ of the time-dependent coherent states reduced by the dipole interaction. These are two spheres of the $\hat{n}$ vectors in the NPD and HPD. The north poles of the spheres, N_1 and N_2, where $\hat{n}_1=\hat{n}_2=\hat{z}$, are equivalent to each other, as are the south poles $S_1=S_2$, where $\hat{n}_1=\hat{n}_2=-\hat{z}$. c) Universal covering space over $R(S^2,S^2)$, which is a chain of infinite number of spheres.

Both NPD and HPD belong to the same space $\tilde{R}_D$ of degenerate states. Further reduction of symmetry by other, smaller, interactions discriminates between HPD and NPD. Which state is preferable depends on the sign and the magnitude of $\omega - H_0$, on the presence of the counterflow, and on the boundary conditions, as will be discussed in Sec. 3 where the additional orientational energies are considered. The competition between these factors leads to the spatial separation of the HPD and the NPD regions with the phase boundary between them at which $\hat{n}_1 = \hat{n}_2 = \pm\hat{z}$. This can be considered as the boundary conditions at the phase boundary.

The complicated order parameter space with the hierarchy of the length scales results in numerous topologically stable objects and textures in the fields of $\hat{R}^{(1)}$ and $\hat{R}^{(2)}$ matrices.

3. ENERGETICS OF COHERENT STATES

3.1. Spectroscopic energy

An additional orienting energy term appears if $\omega \neq \mathbf{H}_0$. In this case the Larmor energy—$\mathbf{H}_0 \cdot \mathbf{S}$ is not compensated completed by the precession and one has the term

$$F_\omega = (\omega - \mathbf{H}_0)\cdot\mathbf{S} = \chi_B(\omega - \mathbf{H}_0)\cdot\hat{R}^{(1)}\mathbf{H}_0, \qquad (3.1)$$

where we have used Eqs. (2.6) and (2.7) for the spin [see also Appendix C where this term, Eq. (C2), is obtained from the Lagrangian for the spin dynamics]. This is the so-called spectroscopic energy, which depends only on the $\hat{R}^{(1)}$ matrix. In different notation it was introduced by Fomin (see Ref. 18). Due to the violation of Z_2 symmetry for $\omega \neq \omega_L$ this term discriminates between HPD and NPD states.

Usually in experimental situations this term is small compared to the dipole interaction. In the limit of extremely large dipole coupling one can assume that at each point of the vessel we have either the HPD state $[\hat{R}^{(2)} = 1$ and $\hat{R}^{(1)} = \hat{R}^{(1)}(\hat{n}_1, \theta_0)]$ or the NPD state $[\hat{R}^{(1)} = 1$ and $\hat{R}^{(2)} = \hat{R}^{(2)}(\hat{n}_1, \theta_0)]$.

For the NPD state, where $\mathbf{S} = \chi_B \mathbf{H}_0$, the spectroscopic energy

$$F_\omega(NPD) = \chi_B(\omega - \mathbf{H}_0)\cdot\omega = \chi_B\omega(\omega - H_0) \qquad (3.2)$$

does not depend on the orientation of $\hat{n}_2$. On the other hand for the HPD state it depends on the orientation of $\hat{n}_1$:

$$F_\omega(HPD) = \chi_B\omega(\omega - H_0)R^{(1)}_{zz}$$

$$= \chi_B\omega(\omega - H_0)(\cos\theta_0 + n_{1z}^2(1 - \cos\theta_0)), \qquad (3.3)$$

and the equilibrium orientation of $\hat{n}_1$ is defined by the sign $\omega - H_0$.

If $\omega - H_0$ is negative, then $\hat{n}_1^{eq} = \pm\hat{z}$, which means that the NPD state is preferable. Since the NPD energy does not depend on the orientation of $\hat{n}_2$, the $\hat{n}_2$ vector in the NPD state is arbitrary (here and below we neglect the very small interaction of $\hat{n}_2$ with $\mathbf{H}_0$). Therefore, if $\omega - H_0$ is negative, the space $R(S^2_{\mathrm{HPD}}, S^2_{\mathrm{NPD}})$ (the bundle of the two spheres of $\hat{n}_1$ and $\hat{n}_2$) is further reduced to a single S^2_{NPD} sphere of $\hat{n}_2$ of NPD.

For positive $\omega - H_0$ the $\hat{n}_1$ vector in the equilibrium is constrained to be in the plane transverse to $\hat{z}$, as follows from Eq. (3.3), which now requires that $\hat{n}_{1z} = 0$. Since the equilibrium HPD energy in this case is less than the NPD energy

$$F_\omega(HPD) - F_\omega(NPD) = -\chi_B\omega(\omega - H_0)(1 - \cos\theta_0), \qquad (3.4)$$

the HPD state takes place in the equilibrium. As a result, for $\omega > H_0$ the space $R(S^2_{\mathrm{HPD}}, S^2_{\mathrm{NPD}})$ of $\hat{n}_1$ and $\hat{n}_2$ is reduced to the S^1 space of $\hat{n}_1$ in the transverse plane. This is the circumference of the precession phase α_1 in the HPD, which gives rise to vortices with $2\pi N$ winding of α_1 (Refs. 7, 9). According to Eq. (2.8) the tipping angle β_1 of the precessing spin in the equilibrium HPD

$$\hat{s}_z = \cos\beta_1 = R^{(1)}_{zz} = \cos\theta_0 = -1/4$$

coincides with the angle θ_0.

If the spectroscopic energy is not infinitely small compared to the dipole energy, then both energy terms (2.12) + (3.3) should be minimized, and one obtains for the equilibrium values of $\hat{s}_z$ and θ:

$$\hat{s}_z = \cos\theta = -\frac{1}{4} - \frac{15}{16}\frac{\omega(\omega - \omega_L)}{\Omega_L^2}.$$

It is instructive to see what occurs if $\omega(\omega - H) \gg \Omega_L^2$; i.e., the dipole forces are small compared to the spectroscopic energy and can be neglected. In this case for $\omega > H_0$ the precessing state is preferable with $n_{1z} = 0$ and $\cos\theta_1 = -1$, which means that the magnetization is opposite to the field direction $\mathbf{S} = -\mathbf{H}_0$. The remaining degeneracy space of this reversed spin state (RSD) is the SO_3 space of the $\hat{R}^{(2)}$ matrix. This space is further reduced by the dipole interaction, which gives $\hat{l}_z = 0$.

3.2. Counterflow effect

In contrast with the spectroscopic term, the counterflow interacts with the orbital vector $\hat{l}$ due to the anisotropy of the superflow along $\hat{l}$, and so the counterflow term in the energy depends only on the $\hat{R}^{(2)}$ matrix:

$$F_u = -1/2\rho_a(\mathbf{u}\cdot\hat{l})^2 = -1/2\rho_a(\mathbf{u}\cdot\hat{R}^{(2)}\cdot\hat{z})^2, \qquad (3.5)$$

where $\mathbf{u} = \mathbf{v}_s - \mathbf{v}_n$ and ρ_a is the anisotropy of the superfluid density along and perpendicular to $\hat{l}$ (see, e.g., Ref. 19).

Let us consider the effect of the counterflow in the limit of strong dipole interaction. For the HPD state, where $\hat{l} = \hat{z}$, this term

$$F_u(HPD) = -1/2\rho_a(\mathbf{u}\cdot\hat{z})^2 \qquad (3.6)$$

does not depend on the orientation of $\hat{n}_1$ and is exactly zero if $\mathbf{u} \perp \mathbf{H}_0$. On the other hand, for the NPD state one has Eq. (3.5), which orients the $\hat{n}_2$ vector in such a manner that this energy is minimized. So in the equilibrium NPD state under the counterflow we have

$$F_u(NPD) = -1/2\rho_a u^2. \qquad (3.7)$$

Hence this term always makes the equilibrium NPD state more advantageous, since

$$F_u(\mathrm{NPD}) - F_u(HPD) = -1/2\rho_a(\mathbf{u}\times\hat{z})^2 < 0. \qquad (3.8)$$

As a result, due to the counterflow (if the counterflow effect dominates the spectroscopic term) the whole space $R(S^2_{\mathrm{HPD}}, S^2_{\mathrm{NPD}})$ of $\hat{n}_1$ and $\hat{n}_2$ vectors is reduced to two or four discrete points of $\hat{n}_2$ which correspond to the minimum of the counterflow energy.

If the counterflow effect and the spectroscopic term are comparable to the dipole energy, the equilibrium state is ob-

tained by the minimization of all three energy terms:

$$F = F_u + F_\omega + F_D = -{}^1/_2\rho_a(\mathbf{u}\cdot\hat{l})^2 + \chi_B\omega(\omega - H_0)\hat{s}_z + {}^2/_{15}\chi_B\Omega_L{}^2[(\hat{s}_z\hat{l}_z - {}^1/_2 + {}^1/_2(1+\hat{s}_z)(1+\hat{l}_z)\cos\gamma)^2 + {}^1/_8(1-\hat{s}_z)^2(1-\hat{l}_z)^2 + (1-\hat{s}_z{}^2)(1-\hat{l}_z{}^2)(1+\cos\gamma)].$$

For $\mathbf{u}\perp\mathbf{H}_0$ this leads to the phase diagram in the u, $(\omega - H_0)$ plane with three phases, HPD, NPD and RSD, with the first order transition lines between the states.[20]

3.3. Surface energy at the container wall and boundary conditions

The surface energy also depends only on the $\hat{R}^{(2)}$ matrix:

$$F_s = -dH_0{}^2(\hat{\nu}\cdot\hat{l})^2 = -dH_0{}^2(\hat{\nu}\cdot\hat{R}^{(2)}\cdot\hat{z})^2. \tag{3.9}$$

Therefore it also leads to the preference of the NPD state in which $\hat{l}$ can be oriented along the normal $\hat{\nu}$ to decrease the surface energy. This gives the boundary conditions for the NPD state if the surface energy is large enough. For the HPD state, where $\hat{l} = \hat{z}$, this term

$$F_s(HPD) = -dH_0{}^2(\nu\cdot\hat{z})^2 \tag{3.10}$$

does not depend on the orientation of $\hat{n}_1$, and there are therefore no boundary conditions for $\hat{n}_1$.

3.4. Gradient energy

The gradient energy should be written in terms of the degeneracy parameters $\hat{R}^{(1)}$ and $\hat{R}^{(2)}$. It can be obtained by substituting Eq. (2.5) into the conventional gradient energy of the B-phase:

$$F_{grad}(\hat{R}) = {}^1/_4\chi_B c_\parallel{}^2(\nabla_i R_{\alpha k})^2 + {}^1/_2\chi_B(c_\parallel{}^2 - c_\perp{}^2)(\nabla_i R_{\alpha i})^2. \tag{3.11}$$

The simplest expression is obtained in the limit of the large dipole energy which fixes either the HPD or the NPD states. For the NPD family the gradient energy has a conventional form:

$$F_{grad}(NPD) = \chi_B c_\perp{}^2(1-\cos\theta_0)(\partial_i\hat{n}_2)^2 - {}^1/_2\chi_B(c_\perp{}^2 - c_\parallel{}^2)(\sin\theta_0\nabla\cdot\hat{n}_2 + (1-\cos\theta_0)\hat{n}_2\cdot\nabla\times\hat{n}_2)^2. \tag{3.12}$$

For the HPD states the Eq. (3.11) should be averaged over the precession period to obtain the gradient energy in terms of the $\hat{n}_1$ vector in the precessing frame:

$$F_{grad}(HPD) = \chi_B c_\perp^2(1-\cos\theta_0)(\partial_i\hat{n}_1)^2 - {}^1/_4\chi_B(c_\perp^2 - c_\parallel^2)[(\sin\theta_0\nabla\cdot\hat{n}_1 + (1-\cos\theta_0)\hat{n}_1\cdot\nabla\times\hat{n}_1)^2 + (\sin\theta_0\nabla_z\hat{n}_{1z} + (1-\cos\theta_0)\hat{n}_1\cdot\hat{z}\times\nabla_z\hat{n}_1)^2 + \sin^2\theta_0(\hat{z}\cdot\nabla\times\hat{n}_1)^2]. \tag{3.13}$$

The gradient energy produces the healing lengths for different interaction. For example the healing length for the spectroscopic energy term is

$$\xi_\omega = \frac{c_\parallel}{[\omega(\omega - H_0)]^{1/2}}.$$

3.5. HPD–NPD interface

The two domain precession discovered in Refs. 1–4 has been extensively investigated both theoretically and experimentally, including the influence of the counterflow on the position and structure of the domain boundary.[19] Here we discuss this in terms of the $\hat{n}_1$ and $\hat{n}_2$ vectors. In some cases this simplifies the problem. The interface between the HPD and the NPD is the surface at which $\hat{n}_1 = \hat{n}_2 = \pm\hat{z}$. This surface is always accompanied by the neighboring textures where the $\hat{n}_1$ and $\hat{n}_2$ vectors are reoriented to obtain the equilibrium orientation far from the interface. Usually the whole texture of the $\hat{n}_1$ and $\hat{n}_2$ vectors on both sides of the interface is called the domain boundary.

To find the structure of the HPD–NPD phase boundary one should solve the separate equations for $\hat{n}_1$ on the HPD side of the interface and for $\hat{n}_2$ on the NPD side with the boundary conditions $\hat{n}_1 = \hat{n}_2 = \pm\hat{z}$ at the interface between NPD and HPD. The equation for $\hat{n}_2$ on the NPD side is obtained by minimizing

$$F(NPD) = F_{grad}(NPD) + F_s(NPD) + F_u(NPD), \tag{3.14}$$

while the equation for $\hat{n}_1$ on the HPD side is obtained by minimizing

$$F(HPD) = F_{grad}(HPD) + F_\omega(HPD). \tag{3.15}$$

The solution of these equations gives the $\hat{n}_1$ and $\hat{n}_2$ textures outside the interface. These textures depend on the position of the interface, so the final step is to minimize the obtained total energy $F(\text{HPD}) + F(\text{NPD})$ as a function of the interface position to find the equilibrium position of the interface.

Sometimes the problem of the equilibrium position of the interface is simplified. The interface is obtained as the surface at which the force from the HPD domain is compensated by the force from the NPD domain; i.e., the energy densities of the states become equal:

$$F_\omega(HPD, \mathbf{r}) + F_u(HPD, \mathbf{r}) = F_\omega(NPD, \mathbf{r}) + F_u(NPD, \mathbf{r}). \tag{3.16}$$

This corresponds to the coexistence of the phases separated by the first-order transition line. Equation (3.16) is valid if the forces are large enough, and so the characteristic lengths of the $\hat{n}$ textures are small compared with the characteristic length scales at which the orientational energies change. The Eq. (3.16) gives the following equation for the interface position in the presence of inhomogeneous magnetic field and superflow:[19]

$${}^5/_4\chi_B\omega(\omega - H_0(\mathbf{r})) = {}^1/_2\rho_a(\mathbf{u}(\mathbf{r})\times\hat{z})^2. \tag{3.17}$$

The $\hat{n}_1$ and $\hat{n}_2$ textures of the HPD–NPD interface in the presence of the counterflow were calculated in Ref. 20.

4. SMALL-SCALE TOPOLOGY OF LARMOR PRECESSION

4.1. Homotopy groups

The topology of the Larmor precession at distances $< \xi_D$ is given by the order parameter space $\tilde{R}$ in Eq. (2.11) with the following homotopy groups:

$$\pi_1(\tilde{R}) = Z_2 \times Z, \tag{4.1}$$

$$\pi_2(\tilde{R}) = Z. \tag{4.2}$$

The $\pi_1(\tilde{R})$ group is the same as in the stationary state of the B-phase and gives rise to the quantized vortices and disclinations, while the $\pi_2(\tilde{R})$ group is nontrivial only due to the extension of the B-phase degeneracy space R to the whole space $\tilde{R}$ of coherent precession. It describes the point de-

fects, hedgehogs, with an integer topological invariant; such hedgehogs cannot exist in the stationary case.

4.2. Hedgehog in the spin and orbital vectors

The object with the nontrivial $\pi_2(\tilde{R})$ is the hedgehog in the field $\hat{s}$ in the precessing frame, accompanied by the hedgehog in the field $\hat{l}$ in the laboratory frame. The integer topological invariant of the hedgehog is given by

$$N=\frac{1}{8\pi}\int_\sigma dA_i e_{ijk}\hat{s}\cdot\partial_j\hat{s}\times\partial_k\hat{s}\,, \tag{4.3}$$

where the integration is over the closed surface σ around the hedgehog. The $\hat{l}$ vector has the same invariant:

$$N=\frac{1}{8\pi}\int_\sigma dA_i e_{ijk}\hat{l}\cdot\partial_j\hat{l}\times\partial_k\hat{l}. \tag{4.4}$$

The distribution of the spin and orbital momenta in the spherically symmetric hedgehog with the topological charge $N=1$ is given by

$$\hat{s}(\mathbf{r})=\hat{r},\quad \hat{l}(\mathbf{r})=\hat{r}\,, \tag{4.5}$$

while the order parameter in this spherically symmetric hedgehog is given by

$$\begin{aligned}R_{\alpha i}(t)&=O_{\alpha\beta}(\hat{z},-\omega_L t)O_{\beta i}(\hat{r},\omega_L t)\\&=O_{\alpha\beta}(\hat{z},-\omega_L t)\,[\delta_{\beta i}\cos(\omega_L t)+\hat{r}_\beta\hat{r}_i(1-\cos(\omega_L t))\\&\quad -e_{\beta ik}\hat{r}_k\sin(\omega_L t)]\,.\end{aligned} \tag{4.6}$$

It is important that the $\hat{s}$ and $\hat{l}$ hedgehogs cannot be separated from each other. If the Euler angles α_1 and β_1 have a point singularity, it should be accompanied by the linear singularity in γ_1 attached to the $\hat{s}$ hedgehog: γ_1 has 4π winding around this line. In the same manner, if the Euler angles α_2 and β_2 have a point singularity, it should be accompanied by the linear singularity in γ_2 attached to the $\hat{l}$ hedgehog: γ_2 has a 4π winding around this line. If $\hat{s}$ and $\hat{l}$ hedgehogs are at the same point in space, the physical parameter $\gamma=\gamma_1-\gamma_2$ is well defined everywhere since the singularities in γ_1 and γ_2 compensate each other. So one has the topological confinement of the $\hat{s}$ and $\hat{l}$ hedgehogs. The separation will lead to the singular line connecting the point defects (Fig. 2): on the line the angle γ of the relative z rotations of matrices $\hat{R}^{(1)}$ and $\hat{R}^{(2)}$ is not well defined since it has a 4π winding. This resembles the 4π vortex tail attached to the $\hat{l}$ monopole in the A-phase. The tail gives rise to the attraction of the $\hat{s}$ and $\hat{l}$ hedgehogs.

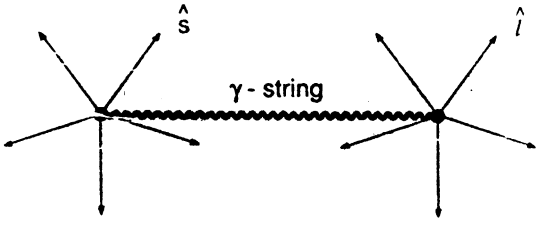

FIG. 2. Small-scale hedgehog in the time-dependent coherent state (illustration of why the constituent $\hat{s}$ and $\hat{l}$ hedgehogs cannot be separated from each other). The disclination line appears between the hedgehogs, which serves as the string confining the monopoles.

5. LARGE DISTANCE TOPOLOGY: DIPOLE INTERACTION

5.1. Bunch of domains (interfacial vortices)

The dipole forces reduce the degeneracy space to the $\tilde{R}_D$ space of HPD and NPD. The first homotopy group of this reduced space is

$$\pi_1(\tilde{R}_D)=Z\times Z, \tag{5.1}$$

while in the stationary case

$$\pi_1(R_D)=Z. \tag{5.2}$$

The additional fundamental homotopy group Z in $\pi_1(\tilde{R}_D)$ comes from the existence of two points in $\tilde{R}_D$ where the spheres S^2_{HPD} and S^2_{NPD} touch each other. Such a bundle of spheres corresponds to a torus with two opposite circumferences contracted to points. The nontrivial topology of such a torus gives rise to the singular line with integer charge $\tilde{N}$. This singular line represents the bunch of the boundaries between NPD and HPD.

A singular line with $\tilde{N}=1$ (Fig. 3a) can be also considered as a linear singularity of the HPD–NPD interface (linear boojum). In accordance with Ref. 21, where the general classification scheme for the defects on the interface between different phases of ordered media has been constructed, this line represents the nontrivial element of the relative homotopy group $\pi_1(S^2_{\mathrm{HPD}}\times S^2_{\mathrm{NPD}},Z_2)=\pi_0(Z_2)=Z_2$. Here S^2_{HPD} and S^2_{NPD} are spheres of vectors $\hat{n}_1$ and $\hat{n}_2$ respectively outside the interface, and Z_2 stands for two possible orientations of $\hat{n}_1=\hat{n}_2=\pm\hat{z}$ on the boundary, which characterize the two-fold degeneracy of the interface (Fig. 3b).

Larger integer $\tilde{N}$s correspond to a bunch of $2\tilde{N}$ interfaces (between HPD's and NPD's) emanating from the singular line (see Fig. 3c for $\tilde{N}=2$). Outside the topologically stable line each of the two neighboring interfaces have opposite directions of $\hat{n}$. Figure 3d illustrates how a singular line with $\tilde{N}>1$ can be decomposed into primitive singularities of the HPD–NPD interface with $\tilde{N}=1$ of Fig. 3a.

5.2. $\hat{n}_1$ and $\hat{n}_2$ hedgehogs

One can show (see Appendix E) that pointlike singularities for the reduced space $\tilde{R}_D$ are classified by two integer indices. Instead of one type of $\hat{n}$ hedgehogs in the stationary state, the order parameter space gives rise to $\hat{n}_1$ hedgehogs in the precessing frame within the HPD and to conventional $\hat{n}_2$ hedgehogs within the NPD. A typical example of an $\hat{n}_1$ hedgehog within the HPD is $\hat{n}_1=\hat{r}$ in the rotating frame while a typical example of an $\hat{n}_2$ hedgehog within the NPD is $\hat{n}_2=\hat{r}$ in the laboratory frame. The angle $\theta=\theta_0$ at $r>\xi_D$ and $\theta\to 0$ at $r\to 0$. The distribution of the spin density for the hedgehog within HPD is given by:

$$\begin{aligned}\hat{s}(\mathbf{r})=\hat{R}^{(1)}(\hat{n}_1(r),\,\theta_0)\,\hat{z}&=\hat{z}\cos\theta_0+\hat{r}\,(1-\cos\theta_0)\cos\tilde{\theta}\\&\quad-\hat{\varphi}\sin\theta_0\sin\tilde{\theta},\end{aligned} \tag{5.3}$$

where r, $\tilde{\theta}$ and φ are spherical coordinates.

The hedgehogs cannot penetrate the domain boundary due to the boundary condition $\hat{n}_1=\hat{n}_2=\pm\hat{z}$.

5.3. The relative homotopy groups: cylindrical domains of magnetization

The relative homotopy groups give rise to the planar and linear solitons. In our case

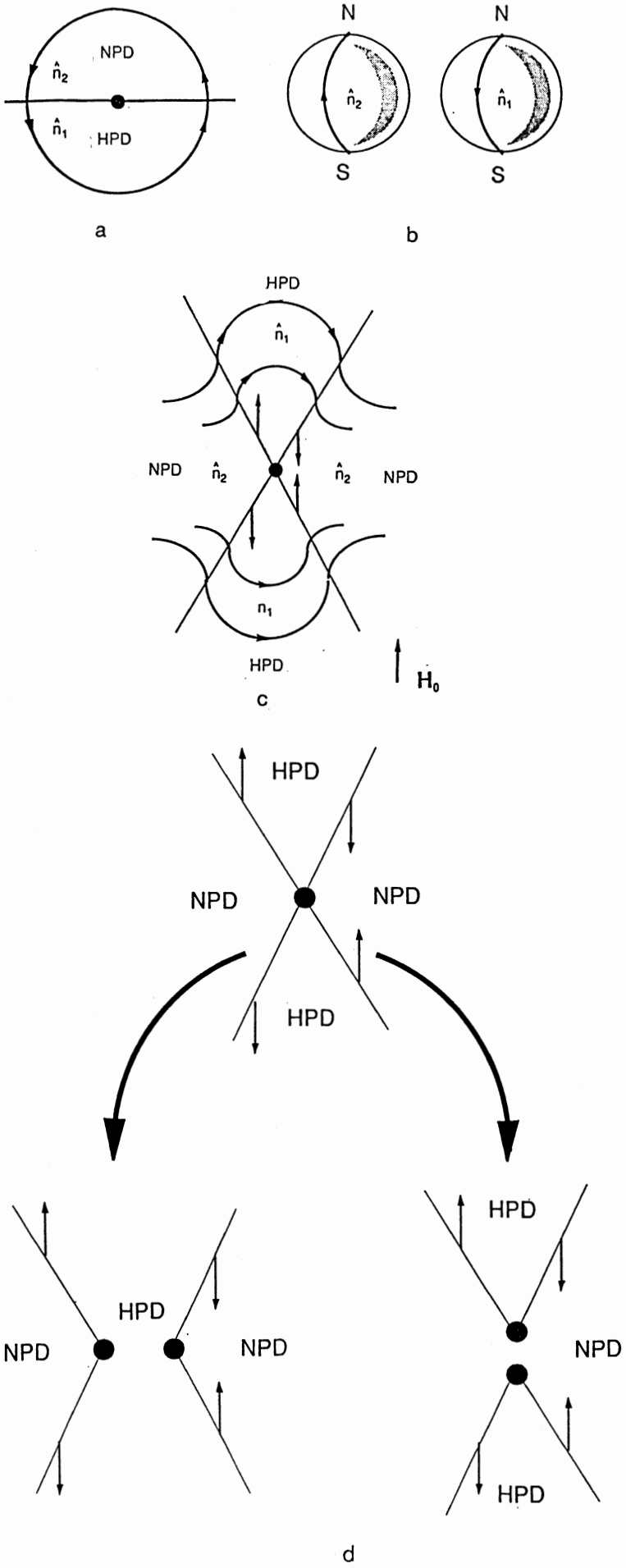

FIG. 3. Interfacial vortex: the bunch of HPD–NPD interfaces. a) Vortex with the topological charge $N = 1$, which is a linear boojum at the HPD–NPD interface; b) the nontrivial contour in $\tilde{R}_D$, which corresponds to this vortex. The contour starts at the point S of the $\hat{n}_2$ sphere, then at the point N it passes to the $\hat{n}_1$ sphere, where it terminates at the starting point S; c) the vortex with the topological charge $N = 2$; d) two ways of the vortex with $N = 2$ can fission into two primitive vortices with $N = 1$.

$$\pi_1(\tilde{R}, \tilde{R}_D)=Z_2, \tag{5.4}$$
$$\pi_2(\tilde{R}, \tilde{R}_D)=Z. \tag{5.5}$$

The π_1 group is the same as in the stationary case and thus gives the θ solitons with thickness of order ξ_D, while the π_2 group is nontrivial, in contrast with the stationary case. It leads to the existence of the linear solitons (the cylindrical domains).

The cylindrical domain is obtained from the hedgehog in the $\hat{s}$ and $\hat{l}$ fields under the action of the dipole forces. Within this domain the spin distribution has an integer topological invariant

$$\frac{1}{4\pi}\int d^2x \hat{s}\cdot\partial_x\hat{s}\times\partial_y\hat{s}\,, \tag{5.6}$$

where the integral is over the cross section of the domain. The $\hat{l}$ vector field has the same invariant in the domain.

5.4. Relative homotopy groups: θ soliton

According to Eq. (5.4) there is only one topologically nontrivial contour in the $\tilde{R}$ space with the ends of the contour being kept in the $\tilde{R}_D$ subspace. The conventional Maki soliton[22] in the NPD state corresponds to this nontrivial contour and can be constructed if one chooses the contour which passes in the space of the $\hat{R}^{(2)}$ matrix with $\hat{R}^{(1)}$ equal to the unit matrix. Inside the Maki soliton with the minimal energy one has $\hat{n}_2\|\hat{\nu}$, where $\hat{\nu}$ is the normal to the soliton wall. The angle θ_2 of the $\hat{R}^{(2)}$ matrix increases from the equilibrium angle θ_0 to π with constant $\hat{n}_2=\hat{\nu}$ and then decreases from π back to θ_0, but with the opposite $\hat{n}_2=-\hat{\nu}$. This object is also referred to as the θ soliton.

The distribution of the $\hat{R}^{(2)}$ and $\hat{R}^{(1)}$ matrices in the θ soliton can be now deformed in such a manner that the same topologically nontrivial contour passes in the space of the $\hat{R}^{(1)}$ matrix, with $\hat{R}^{(2)}$ being equal to the unit matrix. This corresponds to the θ soliton within the HPD state. Within this soliton the angle θ_1 of the $\hat{R}^{(1)}$ matrix increases from the equilibrium angle θ_0 to π constant $\hat{n}_1$ and then decreases from π back to θ_0, but with the opposite $\hat{n}_1$. According to Eq. (2.7) the tipping angle of the spin $\hat{s}$ changes from θ_0 to π and then back to its equilibrium value far from the soliton, but with the phase α_1 of the precession of $\hat{s}$ changed by π. This soliton has higher dipole energy than the soliton within the NPD: $\hat{n}_1$ is constant in the precessing frame, which means that in the laboratory frame it cannot always be oriented along the normal to the soliton wall to minimize the energy of the soliton.

Now let us consider what occurs for $\omega>H_0$ when the HPD state is the equilibrium state outside the soliton. This corresponds to the experimental situation at which the θ solitons have been observed.[6] There are two ways to incorporate the soliton into the HPD (Fig. 4).

(i) In Fig. 4b the pure HPD soliton in the space of the $\hat{R}^{(1)}$ matrix is shown and the magnetic field is along the vertical axis. The $\hat{n}_1$ vector is precessing, so if at some moment this vector is normal to the soliton wall, then after a quarter of the precession period it should be parallel to the wall.

(ii) In Fig. 4c the conventional Maki soliton is present within the NPD region which is separated from the HPD region by the NPD–HPD interface. Between the soliton wall and the interface the $\hat{n}_2$ vector changes its orientation from $\hat{n}_2\|\hat{\nu}$ at the wall to $\hat{n}_2\|\hat{z}$ at the interface. Then on the HPD side the $\hat{n}_1$ vector changes from $\hat{n}_1\|\hat{z}$ to $\hat{n}_1\perp\hat{z}$ far from the interface. These $\hat{n}_2$ and $\hat{n}_1$ textures, which both have thickness of order $\xi_\omega\gg\xi_D$, form the soft core of the soliton.

The second structure seems to be preferable since $\hat{n}_2$ has a proper (normal) orientation within the hard soliton core of order ξ_D, and so the dipole energy is less for the NPD soliton. The NMR experiment shows that just this second structure, the NPD soliton imbedded into the HPD and coated by the NPD–HPD interface, is realized.[6]

6. TOPOLOGY OF COHERENT STATES: SPECTROSCOPIC ENERGY

The spectroscopic energy term at $\omega>H_0$ reduces the space $\tilde{R}_D$ to the circumference $\tilde{R}_\omega=S^1$ of the HPD states. The relative homotopy group

$$\pi_2(\tilde{R}_D, \tilde{R}_\omega)=Z\times Z \tag{6.1}$$

gives rise to the spin vortices and linear $\hat{n}_1$ solitons.

Spin vortices[7-9] are topologically stable linear objects at $\omega>H$ about which the $2\pi N$ winding of the phase α_1 of precession occurs. The core structure of the vortex depends on its symmetry: in the most symmetric vortex $\hat{n}_1$ is always in the transverse plane. Since $\hat{n}_1$ is not well defined on the vortex axis one should have $\theta_1=0$ on the vortex axis, which leads to an increase of the dipole energy within the core of order ξ_D. Such a core is unstable against a vortex with broken discrete symmetry (parity). Within the core of this vortex of the order $\xi_\omega\gg\xi_D$, the angle $\theta_1=\theta_0$ and the $\hat{n}_1$ vector sweeps either the north or the south hemisphere of the sphere $S^2_{\rm HPD}$. This double degeneracy results from the broken parity.

The cylindrical domain is the nonsingular line: outside the domain the $\hat{n}_1$ vector is uniform and perpendicular to $\hat{z}$, while inside the domain $\hat{n}_1$ has the same structure as $\hat{l}$ in the doubly quantized A-phase vortex; i.e., the integral over the cross section of the cylindrical domain

$$N=\frac{1}{4\pi}\int d^2x\hat{n}_1\cdot\partial_x\hat{n}_1\times\partial_y\hat{n}_1 \tag{6.2}$$

is an integer topological charge (unity in the simplest case). This linear soliton can have an end on the $\hat{n}_1$ hedgehog discussed in Sec. 5.2 with the same topological invariant. The integral (6.2) over the cross section of the soft core of the spin vortex is $N=\pm 1/2$.

7. CORE STRUCTURE OF THE SPIN HEDGEHOG: π_3 INSTANTON

The small-scale singular objects, quantized vortices and disclination, are described by the same elements of the homotopy group π_1 as in the stationary B-phase. Therefore in cores of these singularities the B-phase is distorted in a region of order the superfluid coherence length ξ. The spin hedgehog discussed in Sec. 4 is the only singular object whose stability is dictated by the topology of the space $\tilde{R}$ of the coherent precession, while from the point of view of the B-phase space R this object is topologically trivial. This raises the problem of what occurs within the core of the hedgehog. Is it possible to construct a state within the core without distortion of the B-phase state? This is the problem of the interplay of the topological properties of $\tilde{R}$ and R.

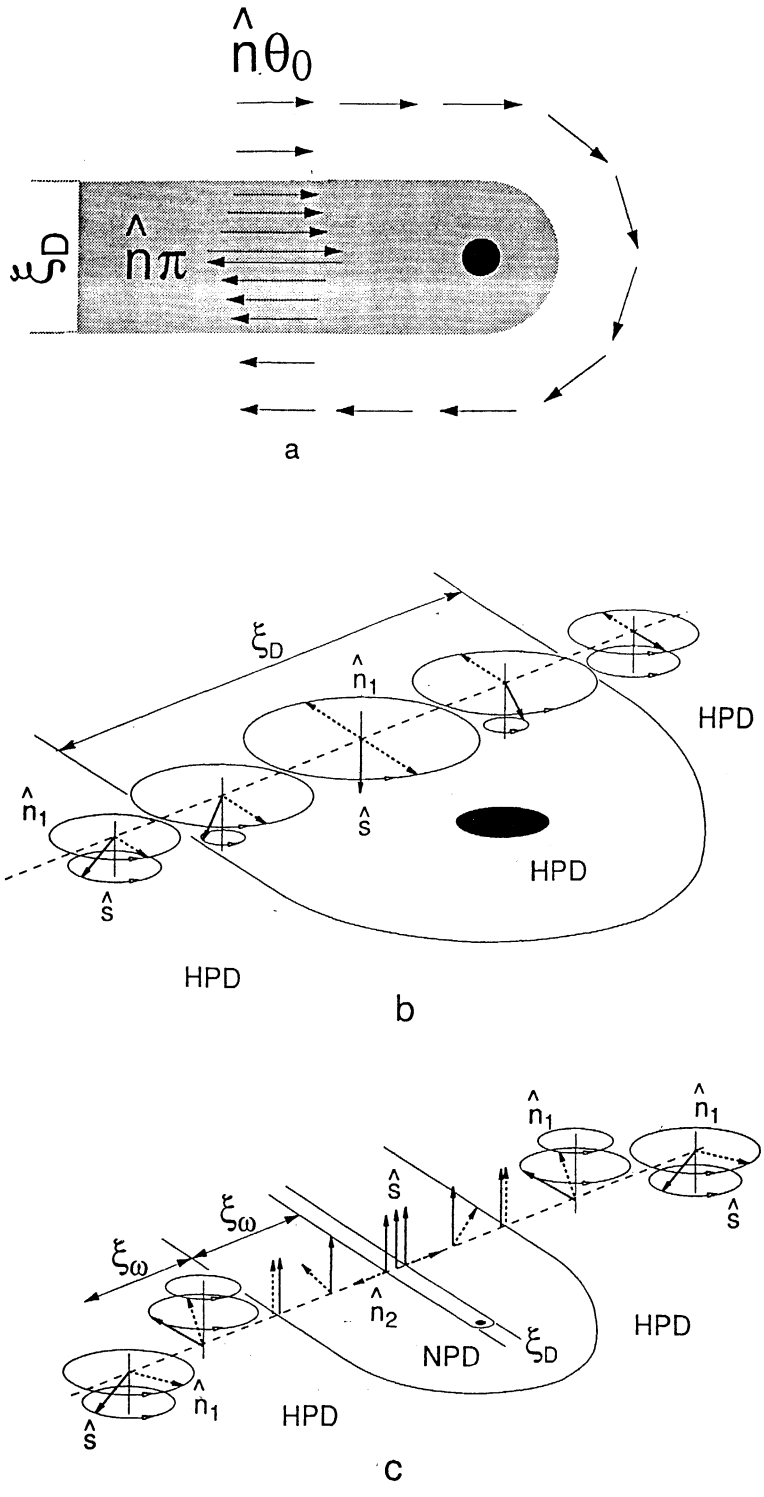

FIG. 4. θ solitons under coherent Larmor precession. a) The distribution of the vector $\hat{n}\theta$ within the conventional soliton wall in the stationary state (NPD); the black dots represent the termination line of the soliton, the θ vortex (disclination). Here $\hat{n}\theta$ changes from $\hat{n}\theta_0$ far from the soliton to the value $\hat{n}\pi$ in the middle of soliton, which is equivalent to $-\hat{n}\pi$. The lowest energy is obtained if all $\hat{n}$ orientations are rotated by $\pi/2$ in the plane of the paper to obtain the normal orientation of $\hat{n}$ within the soliton wall. b) The soliton within the HPD state: HPD penetrates the region of the soliton wall. The spin $\hat{s}$ (solid arrow) is precessing within the soliton wall within the tipping angle which follows the angle θ in Fig. 4a. Therefore the magnetization is reversed in the middle of the soliton compared with its direction in the stationary state. The precession of the $\hat{n}_1$ vector (dashed line) avoids the lowest energy, which is achieved at the normal orientation of $\hat{n}_1$ to the soliton wall. That is why this soliton should be unstable towards the soliton in Fig. 4c. c) Another case of the soliton within the HPD: the HPD does not penetrate the region of the soliton wall, and the soliton is actually within the NPD region separated by the HPD–NPD interface from the HPD in the bulk liquid. The orientation of the $\hat{n}_2$ vector (dashed line) is normal to the soliton wall. The magnetization is stationary within the soliton, being directed along the magnetic field. The NPD and HPD are separated by the HPD–NPD interface. On both sides of interface the $\hat{n}_1$ and $\hat{n}_2$ vectors form the textures of the thickness ξ_ω.

Let us first construct an example of the hedgehog without any singularity in the B-phase order parameter in the core; i.e., the order parameter in the core sweeps the manifold R of the B-phase. It is clear that this spin $\tilde{\mathbf{S}}$ is not well defined at the center of the hedgehog, so the magnitude $S(\mathbf{r})$ of the spin should decrease within the core to zero in the center of the hedgehog. If the gradient energy is neglected then the spherically symmetric solution for the hedgehog including the region of the core is given by

$$R_{\alpha i}(t)=O_{\alpha\beta}(\hat{z},-\omega_L t)\,O_{\beta i}(\hat{r},\omega(\mathbf{r})t)$$
$$=O_{\alpha\beta}(\hat{z},-\omega_L t)\,[\delta_{\beta i}\cos(\omega(\mathbf{r})t)$$
$$+\hat{r}_\beta\hat{r}_i(1-\cos(\omega(\mathbf{r})t))-e_{\beta ik}\hat{r}_k\sin(\omega(\mathbf{r})t)]. \quad (7.1)$$

In this equation the time dependence contains two different frequencies: the Larmor frequency ω_L and the coordinate-dependent frequency $\omega(\mathbf{r})=\chi_B^{-1}S(\mathbf{r})$.

If we now introduce the gradient energy we observe that the gradient energy in Eq. (3.11) diverges with time as t^2 due

to the coordinate dependence of the frequency $S(\mathbf{r})/\chi_B$. This is an example of importance of the stiffness, or rigidity, of the ordered system for HPD: the gradient energy of the order parameter requires the unique coordinate-independent precession frequency. The quantity $\nabla\omega(\mathbf{r})$ for the spin system plays the part of the gradient of the chemical potential for the conventional superflow. It accelerates the spin current, and the quasiequilibrium steady-state spin current is obtained due to periodic phase slip processes. This ac Josephson effect with the spin current was observed within HPD in Ref. 23, where the phase slip process was the unwinding of 2π in the precession angle α.

In our case a similar divergence of the energy also can be stabilized by a kind of ac Josephson effect, when the phase slippage processes reduce periodically the gradient energy. One can conclude that within the core the precession with the homogeneous frequency is violated, but the periodic motion can still survive if the core serves as the source of the periodic phase-slip events. We will see now that in our case the phase-slip process is described by the homotopy group π_3 in contrast with the conventional phase slip described by the homotopy group π_1 of the space of the precession angle α.

Let us show that two possibilities exist: (i) The B-phase with its order parameter matrix $R_{\alpha i}(\mathbf{r},t)$ is well defined everywhere in the core, but the motion is not periodic, since the energy diverges with time. The Eq. (7.1) shows an example of such a situation. (ii) The motion is periodic in time, but at some moments of time there is necessarily a distortion of the B-phase state within the core. This distortion corresponds to the phase slippage center, an instanton, the object in the 4-dimensional space-time with the π_3 topological invariant.

The topology of the dynamical evolution of the order parameter within the core of the hedgehog is defined by the mapping of the 4-dimensional space-time into the order parameter space. Outside the core of the hedgehog the motion is periodic in time; therefore the appropriate space-time manifold surrounding the hedgehog is $S^1\times S^2$, with S^1 being the circumference of the time in the periodic process (see Fig. 5). So outside the core we have some mapping of $S^1\times S^2$ into the space R of the B-phase. We must find out if it is possible to construct a nonsingular solution for the $\hat{R}$ matrix within the core, i.e., without escaping from R. To do this, let us introduce the 3-dimensional solid sphere B^3 of the core volume bounded by S^2 and consider the extension of the mapping of $S^1\times S^2$ into R to the mapping $S^1\times B^3$ into R.

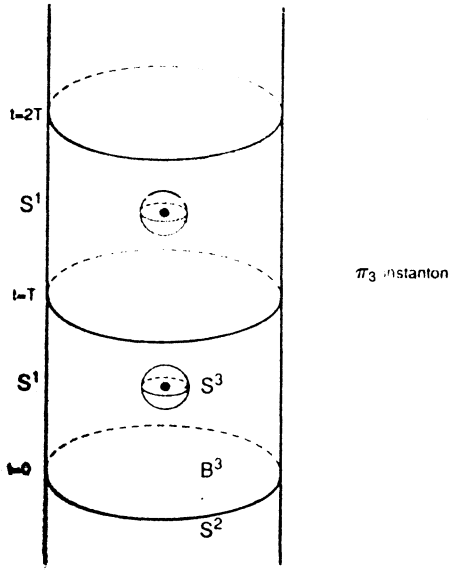

FIG. 5. Topology of the periodic phase slip processes in the core of the spin hedgehog. Each phase-slip event is represented by the instanton, the point in the 4-dimensional time-space $S^1\times B^3$, where B^3 is the core of the hedgehog, and S^1 is the periodic time interval of the length $T=2\pi/\omega_L$. The instanton is described by the integer topological charge of the nontrivial mapping of the three dimensional sphere S^3 around the instanton into the order parameter space SO_3^{rel}.

First we show that the ansatz (4.6) corresponds to the topologically nontrivial mapping of this 3-dimensional space-time $S^1\times S^2$ onto the SO_3^{rel} space of the order parameter matrix $R_{\alpha i}(\hat{r},t)$. The topological invariant (degree of this mapping) can be represented in the form of an integral

$$N=\frac{1}{16\pi^2}\,\mathrm{Tr}\int_0^T dt\int_0^{2\pi} d\varphi\int_0^{\pi} d\tilde{\theta}\,\hat{R}\partial_t\hat{R}^{-1}\hat{R}\partial_\varphi\hat{R}^{-1}\hat{R}\partial_{\tilde{\theta}}\hat{R}^{-1}$$
$$=\frac{1}{16\pi^2}\int_0^T dt\int_0^{2\pi} d\varphi\int_0^{\pi} d\tilde{\theta}\,\partial_t\delta\boldsymbol{\theta}\cdot\partial_\varphi\delta\boldsymbol{\theta}\times\partial_{\tilde{\theta}}\delta\boldsymbol{\theta}, \quad (7.2)$$

where $T=2\pi/\omega$ is the periodic of precession, $\delta\boldsymbol{\theta}$ is the infinitesimal angle of solid rotations of the $\hat{R}$ matrix: $\delta\mathbf{R}_i=\delta\theta\times\mathbf{R}_i$. It follows from the direct calculation that $N=1$ for the ansatz (4.6) describing the hedgehog with unit topological charge (4.3) [in the general case N equals the topological invariant (4.3) of the hedgehog]. This implies that the ansatz (4.6) cannot be continued to get the periodic solution into the entire core volume without escaping from R. Therefore we have either (i) or (ii).

Let us first consider the case (i), the aperiodic process without singularities. Instead of $S^1\times S^2$ of the periodic process we have now $[0,T]\times S^2$—the lateral surface of the 4-dimensional cylinder over B^3 in the space-time whose bases are the core volumes at $t=0$ and $t=T$ (Fig. 5). Topologically the boundary of this cylinder is the sphere S^3. Since we assumed here that there was no singularity in the B-phase matrix $\hat{R}$ within the core, the mapping $S^3\to R$ should be trivial. Hence the integral giving the degree of this mapping vanishes. This integral decomposes into a sum of the integral over the lateral surface (7.2) and the difference of integrals over bases $I_{t=T}-I_{t=0}$. Therefore in the absence of singularities in the B-phase order parameter one has

$$I_{t=T}-I_{t=0}=\frac{1}{16\pi^2}\Big(\int_{t=T} drd\varphi d\tilde{\theta}$$
$$-\int_{t=0} drd\varphi d\tilde{\theta}\Big)\partial\eta\partial\,\boldsymbol{\theta}\cdot\partial_\varphi\delta\boldsymbol{\theta}\times\partial_{\tilde{\theta}}\delta\boldsymbol{\theta}=-1. \quad (7.3)$$

From this equation it follows that as the subsequent times $t=nT$ the integral over the core region is $|I_{t=nT}|=n$; i.e., it increases with time. So this is the aperiodic process (i) in which the core energy increases with time.

For the periodic process (ii) one should have $I_{t=T}=I_{t=0}$, so their difference does not cancel the integral in Eq. (7.2) and the mapping $S^3\to R$ has the winding number $N=1$. This means that there is a singular point in the 4-dimensional space-time of the core where the B-phase order parameter matrix is not well defined. This point, the instan-

ton, has the π_3 topological invariant $N=1$. This number is obtained as the integral in (7.2) taken over the S^3 sphere around the instanton. These instantons realize the phase-slip processes at some times $t_n = t_0 + nT$. In such a process the gradient energy, which monotonically increases with time between the instantons, jumps down. This is the first example of the phase slippage center in condensed matter which is the point in 4-dimensional space-time.

Now we briefly discuss how the transition from the region (i) (the gradient energy growth) to the regime (ii) (the periodic motion) can occur when the inverse gradient approaches the coherent length ξ. If we start with $I_{t=0}=0$ in the process (i), then the evolution of the invariant according to Eq. (7.1) is $|I(t=nT)| \sim n$, and the characteristic gradient is $\sim n^{1/3}/L$, where L is the initial core radius. Thus the transition between the regimes occurs at $n_0 = (L/\xi)^3 \gg 1$. Since the value n_0 at which the phase slip process starts is large, the instanton process of the phase-slip, which leads to $n_0 \to n_0 - 1$, practically does not reduce the gradient energy. This means that in the steady-state periodical regime (ii) with the phase slip, there is a large nonzero average value of the topological invariant $\langle I(t)\rangle \sim n_0$. This corresponds to the nonzero value of the electric current in the ac Josephson effect in superconductors.

The large value of the average topological charge implies that the typical gradients in the core are of order ξ^{-1}; i.e., the hedgehog always has a core of order ξ where the B-phase is distorted. Therefore the phase-slip center is a line in the 4-dimensional space rather than a point. We can construct an example of such a hedgehog with the core radius of order ξ. In order to produce the spherically symmetric state for the hedgehog one can take as the simplest initial state the following stationary spherically symmetric ansatz with zero topological invariant:

$$\mathbf{S}(\mathbf{r}) = \hat{z}H, \quad A_{\alpha i}(\mathbf{r}, t) = f(r)\delta_{\alpha i} \tag{7.4}$$

with $f(r=0)=0$ and $f(r>R_{\text{core}})=1$. Then, applying the topologically nontrivial global spin rotation $\hat{R}^{(1)}(\hat{\varphi},\hat{\theta})$ in the precessing frame and the inverse orbital rotation in the laboratory frame, one obtains the spherically symmetric ansatz with the topological invariant $N=1$ outside the core:

$$A_{\alpha i}(\mathbf{r}, t) = f(r)O_{\alpha\beta}(\hat{z}, -\omega_L t)(\delta_{\beta i}\cos(\omega_L t) + \hat{r}_\beta \hat{r}_i(1-\cos(\omega_L t)) - e_{\beta ik}\hat{r}_k \sin(\omega_L t)). \tag{7.5}$$

This order parameter is well defined at the origin since $f(r=0)=0$.

The function $f(r)$ within the core can be obtained by minimizing the Ginzburg–Landau free energy functional, which for this oversimplified ansatz is reduced to:

$$\int r^2 dr\left(a_1(\partial_r f)^2 + a_2\frac{f^2}{r^2} + (f^2-1)^2\right), \tag{7.6}$$

where the parameters satisfy $a_1 \sim a_2 \sim \xi^2$, and therefore $R_{\text{core}} \approx \xi$.

8. DISCUSSION: LARMOR PRECESSION IN OTHER SUPERFLUID PHASES

The same procedure can be applied for the other phases of superfluid ^{3}He. To consider the precession of the magnetization $\mathbf{S}(t)$ and the axis $\hat{d}(t)$ of the magnetic anisotropy in the A-phase with the frequency close to the Larmor frequency one should start with the initial state, at which the $\hat{d}^{(0)} = \hat{x} \perp \mathbf{H}_0 \| \hat{z}$:

$$A^{(0)}_{\alpha i} = \Delta_A \hat{d}^{(0)}_\alpha (\hat{e}_1 + i\hat{e}_2)_i, \quad \mathbf{S}^{(0)} = \chi_{\perp A}\mathbf{H}_0. \tag{8.1}$$

Application of the symmetry operation SO_3^S of the spin rotations in the precessing frame leads to the following time-dependent $\hat{d}(t)$ and spin:

$$d_\alpha(t) = O_{\alpha\beta}(\hat{z}, -\omega t) R^{(1)}_{\beta\gamma} O_{\gamma\mu}(\hat{z}, \omega t)\hat{d}^{(0)}_\mu, \tag{8.2}$$

$$S_\alpha(t) = O_{\alpha\beta}(\hat{z}, -\omega t) R^{(1)}_{3\gamma}\chi_{\perp A}H_{0\gamma}. \tag{8.3}$$

Thus instead of the sphere S^2 of the $\hat{d}$ vector in the conventional stationary state of the A-phase the precessing states are degenerate over the SO_3 space of the matrix $\hat{R}^{(1)}$ (the spin-orbit interaction is neglected).

This SO_3 space of the $\hat{R}^{(1)}$ matrix is reduced by the spin-orbit dipole interaction:

$$F_D = -g_D(\hat{l}\cdot\hat{d}(t)), \quad \hat{l} = \hat{e}_1 \times \hat{e}_2. \tag{8.4}$$

The equilibrium state chosen by the dipole interaction depends on the angle λ of the $\hat{l}$ vector with respect to magnetic field $\mathbf{H}_0$. This angle can be regulated in the parallel plate geometry.[14] After averaging Eq. (8.4) over the period of precession one has

$$F_D = -\frac{g_D}{8}[\sin^2\lambda((R^{(1)}_{ii} - R^{(1)}_{zz})^2) + 2 + 2(R^{(1)}_{zz})^2) - 4\cos^2\lambda(R^{(1)}_{zz})^2]. \tag{8.5}$$

From Eq. (8.5) it follows that at $\lambda < \pi/4$, the HPD state is preferable to the NPD state. The equilibrium tipping angle of the precessing magnetization is

$$\cos^2\beta = \frac{\sin^2\lambda}{4 - 7\sin^2\lambda}. \tag{8.6}$$

For $\lambda = 0$ the solution for the precessing state was obtained in Ref. 24.

For the larger angles $\lambda > \pi/4$ the NPD is the equilibrium state; i.e, the HPD state is unstable against NPD. This is in agreement with instability of the HPD at $\lambda = \pi/2$, found in the A-phase both theoretically[25] and experimentally.[26] So in the A-phase it is the dipole energy which discriminates between the HPD and the NPD, while in the B-phase the dipole energy is the same for both states and it is the spectroscopic energy term which discriminates between these states.

A similar situation occurs in the A_1-phase, in the A-phase close to the A_1 transition[27] and also in solid ^{3}He.[28]

ACKNOWLEDGMENTS

We thank Yu. M. Bunkov, V. V. Dmitriev, I. A. Fomin, J. S. Korhonen, and M. Krusius for discussions. This work has been supported through the ROTA cooperation plan of the Finnish Academy and the USSR Academy of Sciences.

APPENDIX A

Symmetry of the Lagrangian

The magnetic field plays the part of the time component of the SO_3^S gauge field, so the kinetic term in the Lagrangian expressed in terms of the order parameter field contains the covariant derivative:

$$L=L_{kin}+F(\mathbf{R}_i),\ L_{kin}=-\tfrac{1}{4}\chi_B(D_t\mathbf{R}_i)^2, \tag{A1}$$

where $R_i = R_{\alpha i}$, and the covariant derivative is

$$D_t=\partial_t+\mathbf{H}\times,\ D_t\mathbf{R}_i=\partial_t\mathbf{R}_i+\mathbf{H}\times\mathbf{R}_i. \tag{A2}$$

In the matrix notation

$$D_t=\partial_t-\hat{H},\ D_t\hat{R}=\partial_t\hat{R}-\hat{H}\hat{R},\ H_{\alpha\beta}=e_{\alpha\beta\gamma}H_\gamma \tag{A3}$$

the kinetic term is

$$L_{\rm kin}=-\tfrac{1}{4}\chi_B\,\mathrm{Tr}(D_t\hat{R}D_t\hat{R}^{-1}). \tag{A4}$$

The factor in the kinetic term in Eq. (A1) is chosen so that in the equilibrium state where the order parameter is time-independent, the Lagrangian gives the correct value for the energy of the system in an external magnetic field:

$$L_{\rm eq}=-\tfrac{1}{2}\chi_B H^2+F(\mathbf{R}_i). \tag{A5}$$

The potential energy includes the dipole energy (1.7) and the gradient energy (3.11). In the gradient energy we distinguish here between the isotropic and anisotropic parts:

$$F_{\rm grad}(\hat{R})=F_g^i+F_g^{an}=\tfrac{1}{4}\chi_B c_\parallel^2(\nabla_i R_{\alpha k})^2+\tfrac{1}{2}\chi_B(c_\perp^2-c_\parallel^2)(\nabla_i R_{\alpha i})^2 \tag{A6}$$

[in the Fomin notation we have: $c^2_{\parallel\rm Fomin}=c_1^2$ and $c^2_{1\rm Fomin}=\frac{1}{2}(c_1^2+c_\parallel^2)$].

Different terms in the Lagrangian (A1) have different symmetry.

Local gauge symmetry

The Lagrangian $F_{\rm grad}+L_{\rm kin}$ displays local gauge invariance: the gauge transformation which leaves this Lagrangian invariant,

$$\hat{R}\to\hat{O}(t)\hat{R},\quad \hat{H}\to\hat{O}\hat{H}\hat{O}^{-1}+\partial_t\hat{O}\hat{O}^{-1}, \tag{A7}$$

also includes the change in the magnetic field. Here $\hat{O}(t)$ depends only on t. This invariance is the manifestation of the Larmor theorem, which usually corresponds to special case of gauge transformation: rotation with constant angular velocity

$$\hat{R}\to\hat{O}(\hat{\boldsymbol{\omega}},\omega t)\hat{R},\ \mathbf{H}\to\mathbf{H}-\boldsymbol{\omega}. \tag{A8}$$

The spin-orbit coupling violates the gauge invariances in Eqs. (A7)–(A8).

The following symmetry operations which do not change the magnetic field are important.

Z_2 symmetry

The Lagrangian $F_D+F_g^i+L_{\rm kin}$ displays the following invariance. First we transform

$$\hat{R}\to\hat{O}^{-1}(\hat{z},\omega_L t)\hat{R}\hat{O}(\hat{z},\omega_L t). \tag{A9}$$

At this transformation $F_D+F_g^i$ does not change while the kinetic energy becomes

$$L_{\rm kin}=-\tfrac{1}{4}\chi_B\,\mathrm{Tr}(\tilde{D}_t\hat{R}\tilde{D}_t\hat{R}^{-1}),\ \tilde{D}_t\hat{R}=\partial_t\hat{R}-\hat{R}\hat{H}, \tag{A10}$$

where the covariant derivative is characterized by the matrix $\hat{H}$ on the right, in contrast with the initial energy on the left. To obtain the same Lagrangian this transformation should be supplemented by the transposition of matrix $\hat{R}$, i.e., by the interchange of the spin and orbital indices, and by the substitution $t\to -t$. So the discrete Z_2 symmetry P of the Lagrangian is

$$P\hat{R}(t)=\hat{O}^{-1}(\hat{z},\omega_L t)\hat{R}^{-1}(-t)\hat{O}(\hat{z},\omega_L t) \tag{A11}$$

with $P^2=1$.

This symmetry operation transforms the given NPD state ($\hat{R}^{(1)}=1, \hat{R}^{(2)}=\hat{R}_0$) into the HPD state with $\hat{R}^{(2)}=1$ and $\hat{R}^{(1)}=\hat{R}_0^{-1}$. Therefore most of the properties of the HPD state can be mapped from that of the corresponding stationary state. In particular the collective modes spectrum superposed on the HPD can be obtained from the spin-wave spectrum of the corresponding NPD (see Appendix D). It also transforms the spin degrees of freedom to the orbital ones and vice versa. In particular, the spin density in Eq. (B2) is transformed into the orbital momentum $\mathbf{L}=\hat{R}\mathbf{S}$ in the precessing frame:

$$P\mathbf{S}(t)=\hat{O}^{-1}(\hat{z},\omega_L t)\mathbf{L}(-t),\ P\mathbf{L}(t)=\hat{O}^{-1}(\hat{z},\omega_L t)\mathbf{S}(-t). \tag{A12}$$

The hidden Z_2 symmetry of the Lagrangian results, in particular, from the specific form of the dipole energy, which depends only on the trace of matrix $\hat{R}$. Such a form occurs only in the limit of small ratio $\omega_L/\Delta_B\ll 1$, i.e., when the isotropic B-phase state is not distorted by the magnetic field. For the spatially inhomogeneous case, when the order parameter gradients become important, this invariance is violated by the anisotropic part of gradient energy, which couples the orbital rotation of the matrix $\hat{R}$ with the coordinate transformation.

$\tilde{G}$ SYMMETRY

The Lagrangian $F_g+L_{\rm kin}$ displays the invariance under the global group $\tilde{G}$ in (1.1) which we primarily exploit. The global SO_3^S transformation is

$$\hat{R}\to\hat{O}^{-1}(\hat{z},\omega_L t)\hat{R}^{(1)}\hat{O}(\hat{z},\omega_L t)\hat{R}, \tag{A13}$$

where $\hat{O}(\hat{z},\omega_L t)$ is a rotation with exactly the Larmor frequency about the direction of the field, and $\hat{R}^{(1)}$ is a constant rotation matrix. The global SO_3^L transformation is

$$\hat{R}\to\hat{R}(\hat{R}^{(2)}\mathbf{r})(\hat{R}^{(2)})^{-1}, \tag{A14}$$

where $\hat{R}^{(2)}$ is a constant rotation matrix.

For the most isotropic Lagrangian $F_g^i+L_{\rm kin}$ the SO_3^L transformation extends to $SO_3^{L\,\rm int}\times SO_3^{L\,\rm ext}$, which contains the symmetry $SO_3^{L\,\rm int}$ under the isotopic orbital rotation of matrix $\hat{R}$ and the separate symmetry $SO_3^{L\,\rm ext}$ under the coordinate transformation. The element $g(\hat{R}^{(1)},\hat{R}^{(2)})$ of the symmetry $SO_3^S\times SO_3^{L\,\rm int}$ is thus

$$g(\hat{R}^{(1)},\hat{R}^{(2)})\hat{R}=\hat{O}^{-1}(\hat{z},\omega_L t)\hat{R}^{(1)}\hat{O}(\hat{z},\omega_L t)\hat{R}(\hat{R}^{(2)})^{-1}. \tag{A15}$$

From Eqs. (A15) and (A11) it follows that

$$Pg(\hat{R}^{(1)},\hat{R}^{(2)})P=g((\hat{R}^{(2)})^{-1},(\hat{R}^{(1)})^{-1}). \tag{A16}$$

Dynamic and static symmetries

It is important that the symmetry group of the physical laws could be different for the Lagrangian (A1) and for the

free energy (A5). In the free energy (A5) there is no interaction of the order parameter $\hat{R}$ with the magnetic field due to the isotropy of the magnetic susceptibility of the B-phase in the limiting case of $\omega_L/\Delta_B \ll 1$. The interaction term $-a(\mathbf{H}\cdot\hat{n})^2$ is of order $(\omega_L/\Delta_B)^2\Omega_L^2 \ll \Omega_L^2$ and may be neglected. The interaction between the order parameter and magnetic field appears only at the dynamical level where it is manifested by the covariant derivative in the kinetic term.

APPENDIX B

Leggett equations

The equation obtained from the Lagrangian (A1) is

$$^1/_2 D_t[\chi_B \mathbf{R}_i \times D_t \mathbf{R}_i] = -\frac{\delta F}{\delta \theta}, \quad \frac{\delta F}{\delta \theta} = \mathbf{R}_i \times \frac{\delta F}{\delta \mathbf{R}_i}. \tag{B1}$$

This equation, which is of second order in the time derivative, corresponds to two first order Leggett equations if one introduces the spin density

$$\mathbf{S} = {}^1/_2 \chi_B \mathbf{R}_i \times D_t \mathbf{R}_i. \tag{B2}$$

Substitution of Eq. (B2) into (B1) gives the first Leggett equation for the magnetization:

$$D_t \mathbf{S} = -\frac{\delta F}{\delta \theta}, \tag{B3}$$

while the second Leggett equation for the order parameter is obtained from Eq. (B3) if one solves this equation in favor of $\partial_t \mathbf{R}_i$:

$$\partial_t \mathbf{R}_i = \mathbf{R}_i \times \left(\mathbf{H} - \frac{\mathbf{S}}{\chi_B} \right). \tag{B4}$$

APPENDIX C

Spectroscopic term

The kinetic term in Lagrangian (A1) gives the spectroscopic term (3.1) if $\omega \neq H$. After substitution of Eq. (2.5) with $\omega \neq H$ into the kinetic term of the Lagrangian one obtains

$$D_t \hat{R} = ([^m\omega] - \hat{H})\hat{R} + \hat{O}^{-1}\hat{R}^{(1)}\hat{O}[^m\omega](\hat{R}^{(2)})^{-1},$$

$$L_{\text{kin}} = -{}^1/_2 \chi_B [(\omega - H)^2 + \omega^2]$$

$$-{}^1/_2 \chi_B \operatorname{Tr}([^m\omega] - \hat{H})\hat{R}^{(1)}[^m\omega](\hat{R}^{(1)})^{-1}, \tag{C1}$$

where $[^m\omega]$ is a matrix associated with the vector ω: $[^m\omega]_{\alpha\beta} = e_{\alpha\beta\gamma}\omega_\gamma$. The second term is transformed to

$$F_\omega = \chi_B(\omega - \mathbf{H}_0)\cdot\hat{R}^{(1)}\omega, \tag{C2}$$

which is the so-called spectroscopic term. When ω is close to ω_L this coincides with Eq. (3.1).

APPENDIX D

Collective modes of Larmor precession

The collective modes are the oscillations of the degeneracy parameters $\hat{R}^{(1)}$ and $\hat{R}^{(2)}$ superposed the Larmor precession. If one neglects the anisotropic part of the gradient energy, one can use the Z_2 symmetry in Eq. (A11), which relates the HPD and NPD states. From this symmetry it follows that the spectrum of the collective modes superposed on the HPD is the same as the conventional spectrum superposed on the stationary state if one takes the same condition for the vector $\hat{n}$ in both cases, e.g., $\hat{n} \perp \mathbf{H}$. The spin-wave spectrum superposed on the stationary state is given by equation

$$(\omega^2 - c^2q^2)^3 - (\omega^2 - c^2q^2)^2\Omega_L^2$$

$$-(\omega^2 - c^2q^2)\omega^2\omega_L^2 + \omega^2\omega_L^2\Omega_L^2\hat{n}_z^2 = 0, \tag{D1}$$

where $c = c_\parallel = c_\perp$ for our case of the isotropic gradient energy.

In the limit of small $\Omega_L/\omega_L \ll 1$ one obtains three branches of oscillations on the background of NPD: (i) the branch corresponding to the transverse NMR

$$\omega_{\text{trans}}(\text{NPD}) = \omega_L + \frac{\Omega_L^2\hat{n}_\perp^2 + 2c^2q^2}{2\omega_L}, \tag{D2}$$

(ii) the branch corresponding to the longitudinal NMR

$$\omega_{\text{long}}^2(\text{NPD}) = \Omega_L^2\hat{n}_z^2 + c^2q^2, \tag{D3}$$

and (iii) the branch of the "orbital waves"

$$\omega_{\text{orb}}^2(\text{NPD}) = \frac{c^4q^4}{\omega_L^2}\frac{\Omega_L^2 + c^2q^2}{\Omega_L^2\hat{n}_z^2 + c^2q^2}. \tag{D4}$$

All this coincides with the spectrum of oscillations superposed on HPD found in the precessing frame by Fomin,[16,17] who also observed the similarity in the spin-wave spectrum superposed on the HPD and NPD states. We stress that this similarity is the result of the Z_2 symmetry of the Lagrangian. Under this symmetry operation the orbital and spin vectors, however, are interchanged. This means that the Goldstone modes in the precessing frame are transformed into Goldstone modes in the laboratory frame and vice versa (see Fig. 6). So the spectrum of the orbital waves superposed on the HPD is given by Eq. (D2) with the shifted frequency

$$\omega_{orb}(HPD) = \omega_{trans}(NPD) - \omega_L. \tag{D5}$$

In the same manner

$$\omega_{trans}(HPD) = \omega_{orb}(NPD) + \omega_L. \tag{D6}$$

These oscillations in the background of HPD have been observed.[29,30] And finally, the longitudinal NMR has the same frequency in the precessing and laboratory frames and one obtains

$$\omega_{long}(HPD) = \omega_{long}(NPD). \tag{D7}$$

The Eq. (D5) for the spectrum of the low frequency oscillations of the $\hat{l}$ vector, the orbital waves, superposed on the HPD will be obtained directly now in order to show the consistency of the approach based on the Z_2 transformation. To find the orbital waves let us introduce the time-dependent deviation $\hat{R}^{(2)} - 1$ into the Lagrangian (A1). The main contribution to the kinetic term is given by the first-order term in the time derivative, which in terms of the deviation $\delta\hat{l}$ from the equilibrium value $\hat{l}_{\text{eq}} = \hat{z}$ is

$$L_{\text{kin}}(\hat{l}) = -{}^1/_2 \chi_B(\partial_t \delta\hat{l} \times \delta\hat{l})\cdot\mathbf{H}. \tag{D8}$$

The potential energy is the dipole interaction (2.12), which fixes $\hat{l}_{\text{eq}} = \hat{z}$ in the HPD state, and the gradient energy:

$$F_D(\hat{l}) + F_g{}^i(\hat{l}) = {}^1/_4 \chi_B \Omega_L^2 (\delta\hat{l})^2 + {}^1/_2 \chi_B c^2 (\nabla\delta\hat{l})^2. \tag{D9}$$

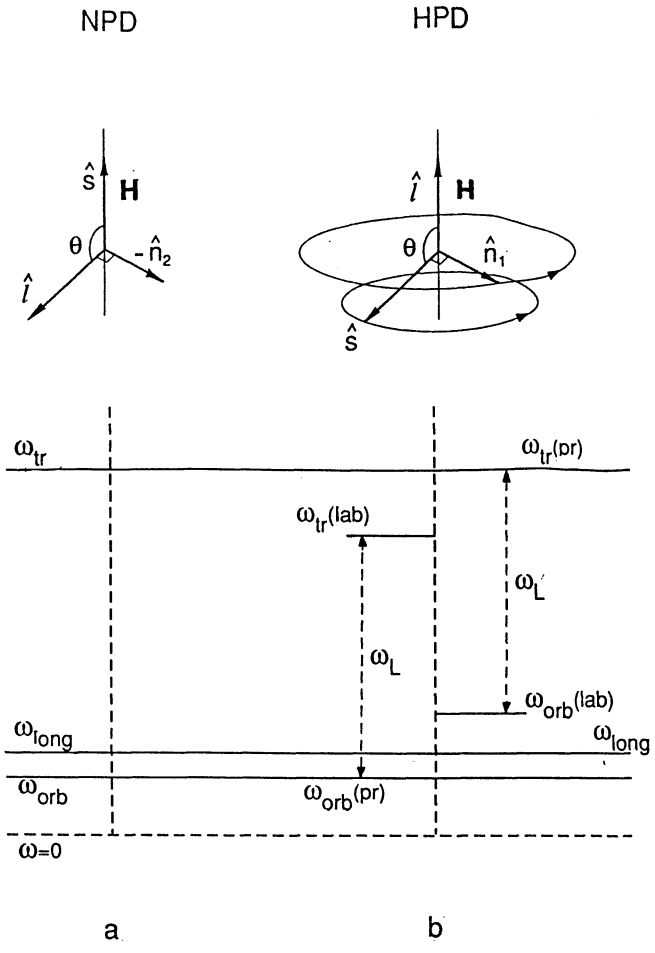

FIG. 6. Schematic presentation of the mapping between the collective modes in the nonprecessing state (NPD, Fig. 6a) and precessing state (HPD, Fig. 6b) caused by the Z_2 symmetry of Lagrangian. If the angle θ between directions of spin $\hat{s}$ and orbital $\hat{l}$ momenta is the same for both states, then the frequencies of the collective modes in the background of the HPD state, considered in the precessing frame (labeled by the letters "pr" in brackets), coincide with the frequencies of spin-wave modes superposed on the corresponding NPD. The frequencies of the HPD excitations measured in the laboratory frame are shifted by the Larmor frequency ω_L, as shown; they are labeled by letters "lab" in brackets.

The variation of $L(\hat{l})$ = (D8) + (D9) leads to the equation for the orbital dynamics of $\hat{l}$:

$$\mathbf{H}\times\partial_t\delta\hat{l}=(^1/_2\Omega_L{}^2+c^2q^2)\delta\hat{l}, \tag{D10}$$

which gives the spectrum of the orbital waves

$$\omega_{\text{orb}}=\frac{\Omega_L{}^2+2c^2q^2}{2\omega_L}. \tag{D11}$$

This coincides with (D5) if one takes $\hat{n}_1^2=1$ in Eq. (D2). The orbital wave spectrum has a dipole gap due to the dipole interaction which fixes the equilibrium $\hat{l}_{\text{eq}}=\hat{z}$ in the HPD.

APPENDIX E

Topology of $\tilde{R}_D$

Here we calculate the homotopy groups for the space $\tilde{R}_D$, which is the total degeneracy space with the dipole interaction taken into account. It follows from (2.13) that the problem can obviously be reduced to that for the bundle $R(S_a^2,S_b^2)$ of two spheres S_a^2 and S_b^2 with two equivalent points $N_1=N_2=N$, $S_1=S_2=S$ (Fig. 1b). The homotopy groups of $R(S_a^2,S_b^2)$ can be calculated with the aid of a universal covering.[11] The universal covering space $\mathscr{C}$ over $R(S_a^2,S_b^2)$ is an infinite chain of spheres

$$\mathscr{C}=\ldots\cup S_{-1}{}^2\cup S_0{}^2\cup S_1{}^2\cup S_2{}^2\cup\ldots,$$

each sphere S_n^2 touches two neighboring ones S_{n-1}^2 and S_{n+1}^2 at the points A_n and A_{n+1} respectively (Fig. 1c). Under the projection of the covering p: $\mathscr{C}\to R(S_a^2,S_b^2)$ the spheres with odd numbers are mapped into (say) S_a^2, while the spheres with even numbers are mapped to another sphere S_b^2. All the points A_{2k+1}, $k\in Z$ are projected to S and the points A_{2k}—to N. One obtains

$$\pi_1(R(S_a{}^2,S_b{}^2))=Z, \tag{E1}$$

the generator σ of this group being represented by a projection of any path γ_1 connecting A_0 and A_2. The element $n\sigma\in\pi_1(R(S_a^2,S_b^2))$ is represented then by a projection of any path γ_k from A_0 to A_{2k}.

Since $\mathscr{C}$ is homotopically equivalent to a bouquet of an infinite number of spheres, the second homotopy group

$$\pi_2(R(S_a{}^2,S_b{}^2))=\pi_2(\mathscr{C})=Z^\infty \tag{E2}$$

turns out to be infinite-dimensional. Apart from the obvious generators α_0 and β_0 represented by the spheres S_a^2, S_b^2 respectively, there arise two series of generators $\alpha_k=\alpha_0+k\sigma$; $\beta_k=\beta_0+k\sigma$ corresponding to projections of all the spheres entering the bouquet $\mathscr{C}$.

In the presence of a linear singularity the turn of a given pointlike singularity transforms it into another one. This transformation is called the action of π_1 on π_2. Equation (E2) does not imply the existence of an infinite number of types of singularities because when π_1 acts nontrivially on π_2 such singularities are classified by the orbits of this action rather than by π_2 itself.[11] In our case the turn around the linear singularity $k\sigma$ transforms the generators of $\pi_2(R(S_a^2,S_b^2))$ as follows:

$$\alpha_0+n\sigma\mapsto\alpha_0+(n+k)\sigma,$$
$$\beta_0+n\sigma\mapsto\beta_0+(n+k)\sigma.$$

Hence this action effectively reduces the number of generators of $\pi_2(R(S_a^2,S_b^2))$ leaving only two integer indices.

[1] A. S. Borovik-Romanov, Yu. M. Bunkov, V. V. Dmitriev, Yu. M. Mukharsky, Pisma Zh. Eksp. Teor. Fiz. **40**, 256 (1984) [JETP Lett. **40**, 1033 (1984)].
[2] A. S. Borovik-Romanov, Yu. M. Bunkov, V. V. Dmitriev *et al.*, Zh. Eksp. Teor. Fiz. **88**, 2025 (1985) [Sov. Phys. JETP **61**, 1199 (1985)].
[3] I. A. Fomin, Pisma Zh. Eksp. Teor. Fiz. **40**, 260 (1984) [JETP Lett. **40**, 1037 (1984)].
[4] I. A. Fomin, Zh. Eksp. Teor. Fiz. **88**, 2039 (1985) [Sov. Phys. JETP **61**, 1207 (1985)].
[5] Y. Kondo, J. S. Korhonen, M. Krusius *et al.*, Phys. Rev. Lett. **67**, 81 (1991).
[6] Y. Kondo, J. S. Korhonen, M. Krusius *et al.*, Phys. Rev. Lett. **68**, 3331 (1992).
[7] I. A. Fomin, Zh. Eksp. Teor. Fiz. **94**, 112 (1988) [Sov. Phys. JETP. **67**, 1148 (1988)].
[8] E. B. Sonin, Pisma Zh. Eksp. Teor. Fiz. **45**, 586 (1987) [JETP Lett. **45**, 747 (1987)].
[9] A. S. Borovik-Romanov, Yu. M. Bunkov, V. V. Dmitriev *et al.*, Physica **B, 165–166**, 649 (1990).
[10] N. D. Mermin, Rev. Mod. Phys. **51**, 591 (1979).
[11] V. P. Mineev, Sov. Sci. Rev. (1980) **A2**, Ed. by I. M. Khalatnikov,

GmbH, Chur, Switzerland: Harwood Acad. Publ., p. 173 (1980).
[12] L. Michel, Rev. Mod. Phys. **52**, 617 (1980).
[13] M. Kléman, *Points, Lines and Walls in Liquid Crystals, Magnetic Systems and Various Ordered Media*, N. Y., Wiley (1983).
[14] D. Vollhardt, and P. Wölfle, *The Superfluid Phases of Helium 3*, Taylor and Francis, London (1990).
[15] M. Liu, Physica B **109–110**, 1615 (1982).
[16] I. A. Fomin, Pisma Zh. Eksp. Teor. Fiz. **28**, 362 (1978). [JETP Lett. **28**, 334 (1978)].
[17] I. A. Fomin, Zh. Eksp. Teor. Fiz. **84**, 2109 (1983) [Sov. Phys. JETP **57**, 1227 (1983)].
[18] I. A. Fomin, *Modern Problems in Condensed Matter Sciences (Helium Three)*, Ed. by W. P. Halperin and L. P. Pitaevskii, North-Holland, 610 (1990).
[19] Yu. M. Bunkov and O. Timofeevskaya, Pisma Zh. Eksp. Teor. Fiz. **54**, 232 (1991) [JETP Lett. **54**, 228 (1991)].
[20] J. S. Korhonen and G. E. Volovik, Pisma Zh. Eksp. Teor. Fiz. **55**, 358 (1992) [JETP Lett. **56**, 362 (1992)].
[21] T. Sh. Misirpashaev, Zh. Eksp. Teor. Fiz. **99**, 1741 (1991) [Sov. Phys. JETP **72**, 973 (1991)].
[22] K. Maki and P. Kumar, Phys. Rev. B **16**, 4805 (1977).
[23] A. S. Borovik-Romanov, Yu. M. Bunkov, A. de Vaard *et al.*, Pisma Zh. Eksp. Teor. Fiz. **47**, 400 (1988) [JETP Lett. **47**, 478 (1988)].
[24] V. L. Golo, Letters Math. Phys. **5**, 115 (1981); Yu. M. Poluektov, Fiz. Nizk. Temp. **10**, 1013 (1984) [Sov. J. Low. Temp. Phys. **10**, 527 (1984)].
[25] I. A. Fomin, Pisma Zh. Eksp. Teor. Fiz. **39**, 387 (1984) [JETP Lett. **39**, 466 (1984)].
[26] A. S. Borovik-Romanov, Yu. M. Bunkov, V. V. Dmitriev, and Yu. M. Mikharsky, Pisma Zh. Eksp. Teor. Fiz. **39**, 390 (1984) [JETP Lett. **39**, 469 (1984)].
[27] G. E. Gurgenishvili and G. A. Kharadze, Pisma Zh. Eksp. Teor. Fiz. **42**, 374 (1985) [JETP Lett. **42**, 461 (1985)].
[28] I. A. Fomin and D. V. Shopova, Pisma Zh. Eksp. Teor. Fiz. **42**, 162 (1985) [JETP Lett. **42**, 199 (1985)].
[29] I. A. Fomin, Pisma Zh. Eksp. Teor. Fiz. **43**, 134 (1986) [JETP Lett. **43**, 171 (1986)].
[30] Yu. M. Bunkov, V. V. Dmitriev, and Yu. M. Mukharsky, Pisma Zh. Eksp. Teor. Fiz. **43**, 131 (1986) [JETP Lett. **43**, 168 (1986)].

Translation submitted by the authors